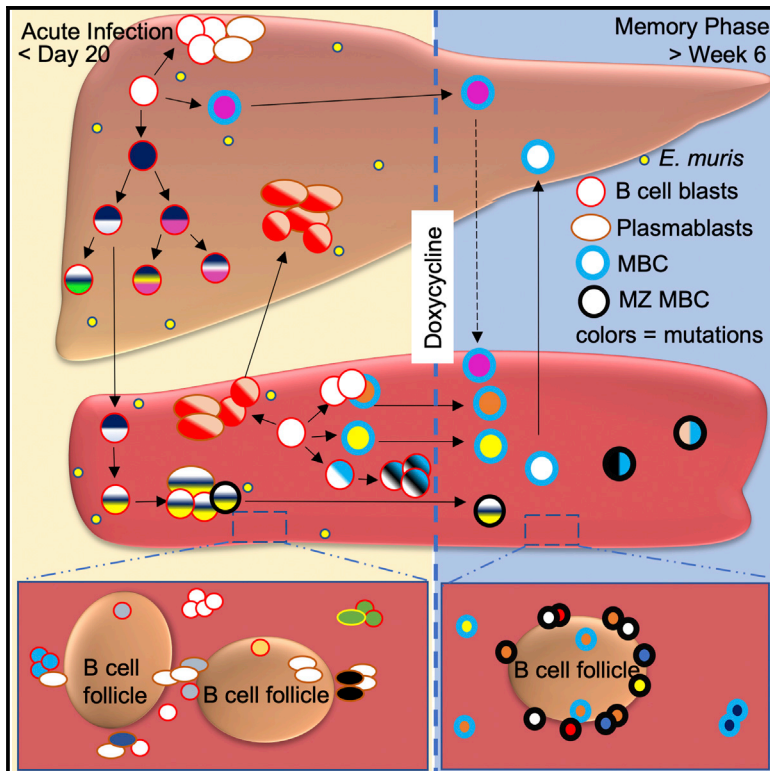


Immunity

Liver Is a Generative Site for the B Cell Response to *Ehrlichia muris*

Graphical Abstract



Authors

Nikita Trivedi, Florian Weisel,
Shuchi Smita, ..., Uri Hershberg,
Nahed Ismail, Mark Jay Shlomchik

Correspondence

mshlomch@pitt.edu

In Brief

Infection by the intracellular bacterium *Ehrlichia* induces few—if any—germinal centers, yet it generates protective immunoglobulin M (IgM) memory B cells (MBCs). Trivedi et al. show that the liver and spleen are generative sites of B cell responses, including V-region mutation and long-term MBC localization, to *E. muris*.

Highlights

- *E. muris* induces localized B cell proliferation, differentiation, and SHM in liver
- Primary response and MBC clones interchange between liver and spleen
- *E. muris* induces T-bet⁺ MBCs that adopt follicular, ABC, and MZ phenotypes
- *E. muris* dissolves the MZ, which is subsequently reconstituted by T-bet⁺ MBCs



Liver Is a Generative Site for the B Cell Response to *Ehrlichia muris*

Nikita Trivedi,^{1,2} Florian Weisel,¹ Shuchi Smita,^{1,6} Stephen Joachim,¹ Muhamuda Kader,³ Aditya Radhakrishnan,⁴ Chris Clouser,⁴ Aaron M. Rosenfeld,⁵ Maria Chikina,⁶ Francois Vigneault,⁴ Uri Hershberg,⁵ Nahed Ismail,³ and Mark Jay Shlomchik^{1,7,8,*}

¹Department of Immunology, University of Pittsburgh, Pittsburgh, PA 15261, USA

²Graduate Program in Microbiology and Immunology, University of Pittsburgh, Pittsburgh, PA 15261, USA

³Department of Pathology, University of Pittsburgh, Pittsburgh, PA 15261, USA

⁴Juno Therapeutics, Seattle, WA 98109, USA

⁵Drexel University, Philadelphia, PA 19104, USA

⁶Department of Computational and Systems Biology, University of Pittsburgh, Pittsburgh, PA 15261, USA

⁷Twitter: @ShlomchikLab

⁸Lead Contact

*Correspondence: mshlomch@pitt.edu

<https://doi.org/10.1016/j.immuni.2019.10.004>

SUMMARY

The B cell response to *Ehrlichia muris* is dominated by plasmablasts (PBs), with few—if any—germinal centers (GCs), yet it generates protective immunoglobulin M (IgM) memory B cells (MBCs) that express the transcription factor T-bet and harbor V-region mutations. Because *Ehrlichia* prominently infects the liver, we investigated the nature of liver B cell response and that of the spleen. B cells within infected livers proliferated and underwent somatic hypermutation (SHM). Vh-region sequencing revealed trafficking of clones between the spleen and liver and often subsequent local clonal expansion and intraparenchymal localization of T-bet⁺ MBCs. T-bet⁺ MBCs expressed MBC subset markers CD80 and PD-L2. Many T-bet⁺ MBCs lacked CD11b or CD11c expression but had marginal zone (MZ) B cell phenotypes and colonized the splenic MZ, revealing T-bet⁺ MBC plasticity. Hence, liver and spleen are generative sites of B cell responses, and they include V-region mutation and result in liver MBC localization.

INTRODUCTION

The conventional B cell response to pathogens such as the influenza virus and the malarial parasite is dependent on a germinal center (GC) pathway that results in the production of antibody-forming cells (AFCs) and memory B cells (MBCs) (Coro et al., 2006; Stephens et al., 2009). However, certain pathogens such as *Borrelia burgdorferi*, *Salmonella typhimurium*, and *Ehrlichia muris* suppress or delay the onset of a GC response; B cell responses instead follow a non-canonical pathway (Hastey et al., 2012; Cunningham et al., 2007; Racine et al., 2010; Di Niro et al., 2015). *Ehrlichia* is a gram-negative, obligate intracellular bacterium that causes a tick-borne infection (Anderson et al., 1991; Dawson et al., 1991). In humans, infection by *Ehrlichia*

chaffeensis causes human monocytotropic ehrlichiosis, which is characterized by flu-like symptoms such as fever, headache, myalgia, and hematological abnormalities (Ismail and McBride, 2017). In both humans and mice, liver is a prominent site of *Ehrlichia* infection (Sehdev and Dumler, 2003; Ismail et al., 2004; Ismail et al., 2010). *Ehrlichia* induces a B cell response in humans, and antibodies (Abs) are detected in the serum of infected patients (Standaert et al., 2000). In mice, *Ehrlichia* infection induces large numbers of immunoglobulin M (IgM) AFCs and considerable, yet comparatively lower, numbers of immunoglobulin G (IgG) AFCs (Racine et al., 2008; Racine et al., 2010; Winslow et al., 2000).

Ehrlichia infection induces the expression of the transcription factor T-bet in AFCs and a subset of splenic MBCs (Winslow et al., 2017). Although T-bet expression in B cells was originally documented as a regulator of isotype switch induced in response to TLR9 signals (Peng et al., 2002; Jegerlehner et al., 2007), it has been closely associated with so-called age-associated B cells (ABCs) (Rubtsov et al., 2011; Hao et al., 2011; Naradikian et al., 2016). ABCs are found especially in older female mice and in autoimmune-prone mice (Hao et al., 2011; Rubtsov et al., 2011). These T-bet⁺ ABCs are typically CD11b⁺ and CD11c⁺ but lack expression of CD21 and CD23 (Hao et al., 2011). A similar population has been identified in humans and is associated with lupus. T-bet⁺ B cells can also be induced by various infections, and T-bet can also be expressed in plasmablasts (PBs). (Rubtsova et al., 2013; Barnett et al., 2016; Moir et al., 2008; Rubtsov et al., 2011; Rubtsova et al., 2017; Rubtsov et al., 2013). A subset of MBCs formed during certain conditions, including *Ehrlichia* infection, can express T-bet as well. The role of T-bet in B cells and its relationship to ABC, MBC, and PB development and function are an active area of research, and the relationships among these cells and processes are not fully clear.

Despite the fact that liver is a primary site for infection in humans and mice (Ismail et al., 2010; Ismail et al., 2004; Sehdev and Dumler, 2003), there is limited information on hepatic B cell responses to *Ehrlichia* (Miura and Rikihisa, 2009; Habib et al., 2016). Here, we examined the extent to which the B cell response to *Ehrlichia* occurs in liver and the consequences of



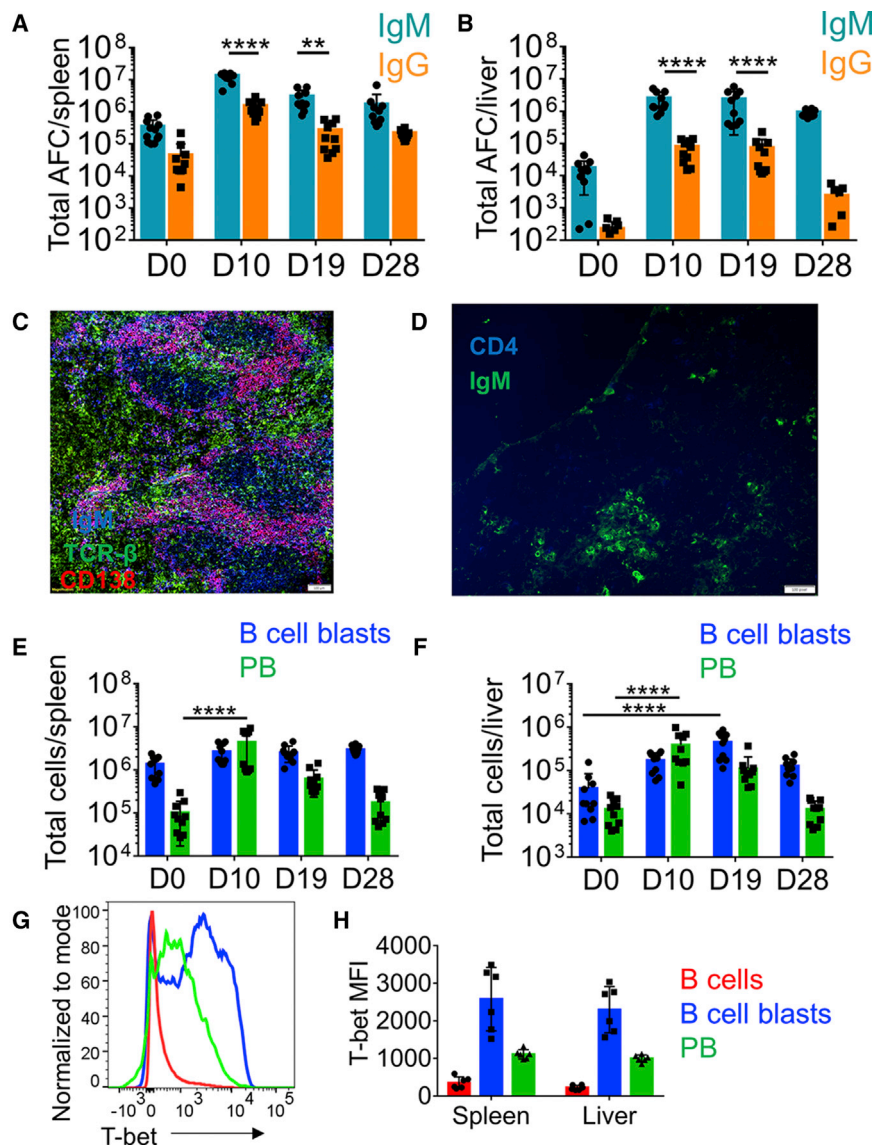


Figure 1. *E. muris* Infection Induces a Robust B Cell Response Marked by T-bet Expression

(A and B) Total IgM and IgG AFCs measured by ELISpot assay during *E. muris* infection in spleen (A) and liver (B).

(C and D) Immunofluorescence staining of cryosections of mouse spleen on day 10 after infection shows PBs (C), and staining of liver cryosections shows B cells and T cells (D). Scale bars represent 100 μ m (C) and 100 pixels (D).

(E and F) Total B cell blasts (blue) and PBs (green) measured by FC over the course of *E. muris* infection in spleen (E) and liver (F).

(G and H) Histogram (G) and mean fluorescence intensity (H) of T-bet expression in B cells during acute *E. muris* infection.

Data are representative of at least 2 independent experiments, and in (A), (B), (E), (F), and (H), data are represented as mean plus SD of groups of at least 2 mice. * $p < 0.05$, ** $p < 0.01$, *** $p < 0.001$, **** $p < 0.0001$. Statistics for (A), (B), (E), and (F) were done by 2-way ANOVA. See Figures S1 and S2.

RESULTS

E. muris Infection Induces a Robust B Cell Response Marked by T-bet Expression

Inoculation of mice with *E. muris* leads to systemic infection of spleen and liver (Ismail et al., 2004; Olano et al., 2004). In response to *Ehrlichia*, splenic B cells do not form GCs and instead respond by rapid extrafollicular expansion (Racine et al., 2010). In agreement with previous reports (Ismail et al., 2004; Olano et al., 2004), we found that *E. muris* infection was marked by a considerable bacterial burden in spleen and liver along with an

this local response. We found that liver was a major locus for B cell proliferation and somatic hypermutation (SHM) during the acute phase of the immune response. High-throughput sequencing (HTS) analyses revealed bi-directional trafficking of mutated B cell blasts and PBs between spleen and liver. After pathogen clearance, we observed T-bet-expressing MBCs that persisted in spleen and were localized in liver, including some that were histologically intraparenchymal and resisted intravascular labeling with intravenous (i.v.) anti-CD19. In spleen, *Ehrlichia* infection remodeled the marginal zone (MZ) compartment, which initially dissolved and was later reconstituted by a majority of T-bet-expressing MBCs induced by infection. Although T-bet-expressing MBC populations have generally been phenotyped as CD11b⁺CD11c⁺CD21[−]CD23[−], many formed after *Ehrlichia* infection have a CD21^{hi}CD23^{lo} MZ phenotype. Further, only a fraction of these are CD11b⁺CD11c⁺. Hence, *Ehrlichia* infection elicits unusual populations of T-bet⁺ MBCs and reveals additional plasticity among these cells.

enlargement of these organs (Figures S1A and S1B). In both spleen and liver, infection elicited large numbers of AFCs by day 10, which remained elevated until at least day 28 after infection (Figures 1A and 1B). There was a substantial IgG response, but the number of IgG AFCs was lower than that of IgM AFCs (Figures 1A and 1B). Responding B cells were located within patches at extrafollicular sites in spleen and in liver parenchyma (Figures 1C and 1D; Figures S1D and S1E). Flow-cytometric analysis of spleen and liver from infected mice revealed expanded populations of B cell blasts (CD44⁺) and PBs (CD44⁺CD138⁺ PBs) (Figure S1F; Figures 1E and 1F). In findings consistent with previous reports (Racine et al., 2010), we did not find induction of PNA⁺ GC B cells by flow cytometry (FC) (Figure S1C). Confirming previous studies (Winslow et al., 2017), we found that PB in *E. muris*-infected mice expressed T-bet. B cell blasts also expressed high amounts of T-bet. (Figures 1G and 1H).

To decipher the role of T-bet in the acute B cell response, we used Tamoxifen-inducible, Cre-mediated deletion of T-bet during an ongoing *E. muris* infection (Figure S2A). Assessment of

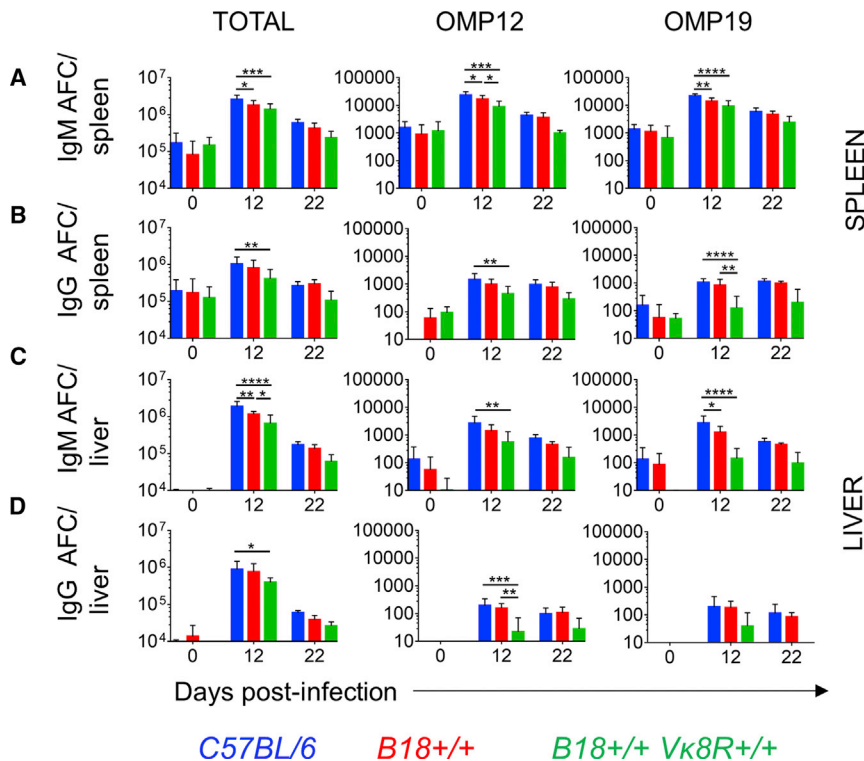


Figure 2. BCR Restriction Reduces the Magnitude of B Cell Response to *E. muris*

(A and B) Total and Ag-specific responses of IgM (A) and IgG (B) to *E. muris* in spleen as measured by ELISpot assay.

(C and D) Total and Ag-specific responses of IgM (C) and IgG (D) to *E. muris* in liver as measured by ELISpot assay.

Data are representative of at least 2 independent experiments and are represented as mean plus SD of groups of at least 2 mice. * $p < 0.05$, ** $p < 0.01$, *** $p < 0.001$, **** $p < 0.0001$. Statistics were done by 2-way ANOVA.

is consistent with non-specific B-cell expansion that is mediated by signals through different pathogen-recognition receptors without relying on B cell receptor (BCR) recognition or stimulation. However, if the B cell response were indeed specific, then restricting the BCR repertoire would negatively affect the AFC response. To examine this, we used (1) heavy-chain-restricted $B18^{+/-}$ mice that utilize B18 heavy-chain genes paired with diverse light chains and (2) heavy- and light-chain-restricted $B18^{+/-}V\kappa8R^{+/-}$

T-bet expression on day 11 after infection revealed that treatment with tamoxifen reduced T-bet expression on splenic B cell blasts and PBs and showed a similar trend in hepatic B cell populations (Figure S2B). Because liver is a metabolically active site, we suspect that tamoxifen was metabolized rapidly by liver cells and was not available for B cells. We assessed the total number of responding B cells and found that splenic PBs were more abundant in T-bet-deficient mice than in the T-bet-sufficient group (Figure S2C). There was no difference in the total numbers of splenic B cell blasts, hepatic B cell blasts, and hepatic PBs upon T-bet deletion (Figure S2C). Enzyme-linked immunosorbent spot (ELISpot) assay showed a trend of increased IgM AFCs in spleen and liver, but there was no difference in total and antigen-specific splenic or hepatic AFCs upon T-bet deletion (Figures S2D–S2I). Unlike what has been observed during influenza infection and lupus disease in mice (Stone et al., 2019; Rubtsova et al., 2017), the *E. muris* AFC response was not dampened in the absence of T-bet. It is possible that even though we did observe lower T-bet expression in responding populations, deletion during B cell development, as performed in the influenza and lupus models, differed from the inducible deletion we performed here.

A Diverse B Cell Receptor Repertoire Is Required for the AFC Response to *E. muris*

We examined the specificity of the responding PBs by using *E. muris* outer-membrane proteins Omp12 and Omp19 as coating antigens (Ags) in ELISpot assays (Crocquet-Valdes et al., 2011). Although these Ags are reported to be immunodominant *E. muris* Ags (Racine et al., 2008; Yates et al., 2013), we found that fewer than 1% of IgM and IgG AFCs were specific to these Ags in both spleen and liver (Figures 2A–2D). This result

mice that utilize B18 heavy-chain and $V\kappa8R$ light-chain genes. In general, we observed a trend of a lower total and Ag-specific AFC response in spleens and livers of the BCR-restricted mice than in those of wild-type (WT) counterparts (Figure 2). In spleen, we observed that heavy- and light-chain restriction led to reduced total, Omp12, and Omp19 AFCs at day 12 after infection (Figures 2A and 2B). The splenic total and Ag-specific IgM AFCs were also reduced merely by heavy-chain restriction at day 12 after infection (Figure 2A). The hepatic total numbers of IgM and IgG AFCs, Omp12-specific IgM and IgG AFCs, and Omp19-specific IgM AFCs were lower in $B18^{+/-}V\kappa8R^{+/-}$ mice than in WT mice at day 12 after infection (Figures 2C and 2D). In all scenarios, BCR-restricted mice mounted an increased response in comparison to baseline but failed to mount an AFC response that matched the magnitude of the WT repertoire (Figure 2). No differences were observed in the AFC response between WT and BCR-restricted mice at day 22 after infection because the acute response had subsided (Figure 2). These data demonstrate that Ag sensing through the BCR is required for the massive AFC response that is seen upon *E. muris* infection and suggest that although the response might be of low affinity, the majority of it depends on specific BCR recognition.

Localized Proliferation and SHM of B Cells in Liver

Although increased numbers of B cell blasts and PBs were found in livers of *E. muris*-infected mice, it was not clear whether the hepatic B cell response was a product of infiltrating B cells derived from lymphoid organs or from local proliferation and differentiation of B cells in liver. To investigate this, we injected the mice with 5-ethynyl-2'-deoxyuridine (EdU) 30 min prior to the harvest of organs so that we could label cells that were actively undergoing DNA synthesis during that period. As expected,

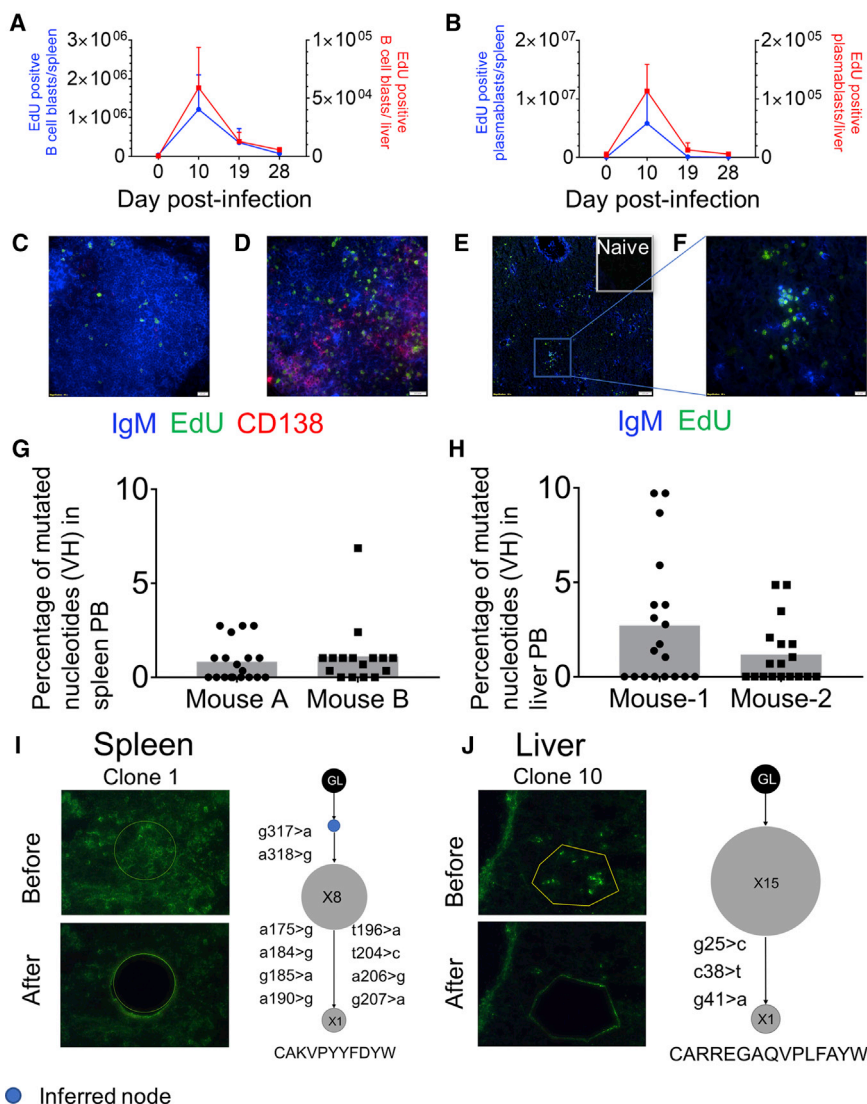


Figure 3. Localized Proliferation and SHM of B Cells in Spleen and Liver

(A and B) EdU⁺ B cell blasts (A) and PB (B) of spleen (blue) and liver (red) over the course of infection as measured by FC.

(C and D) 40 \times image of proliferating B cells in naive spleen (C) and in *E. muris*-infected spleen on day 10 after infection (D).

(E and F) 10 \times (E) and 40 \times (F) images of proliferating B cells in liver parenchyma on day 10 after infection.

(G and H) Percentage of mutated nucleotides in PBs from spleen (G) and liver (H).

(I and J) Laser microdissections of IgM⁺ PB patches (green) and corresponding clonal trees from Ig-region sequencing from spleen (I) and liver (J). Inferred nodes are blue. Node size is proportional to the number of sequences. The CDR3 amino acid sequence of each clone is shown at the bottom.

Data are representative of at least 2 independent experiments. Scale bars represent 20 μ m (C and F), 200 pixels (D), and 100 μ m (E). See Figure S3 and Table S1.

were unmutated at both sites (Figures 3G and 3H), indicating that the cells harboring these did not induce the SHM program. Mutated PBs could either be generated during local proliferation or undergo mutation at a separate site and then migrate. Because we knew that liver is a generative site, we hypothesized that mutation could occur within locally responding foci. To address where mutations were actually occurring, we used laser microdissection of IgM patches from the liver and spleen parenchyma. These microdissections typically captured \sim 20 cells, of which the full nucleus would be present

there were substantially more EdU⁺ splenic B cell blasts and PBs than naive controls 10 days after infection (Figures 3A and 3B). Hepatic B cell blasts and PBs were proliferating to an extent comparable to that of the splenic responders (Figures 3A and 3B). Histologic analysis showed that proliferation of IgM⁺ and CD138⁺ B cells in spleen occurred within and outside of B cell follicles (Figures 3C and 3D; Figure S3A). Proliferation of IgM⁺ B cells in liver was seen in liver parenchyma and around the portal triads (Figures 3E and 3F; Figure S3B). These data indicate that liver is a generative site for the B cell response to *E. muris*.

To investigate the presence of SHM in PB responses that lacked GCs, we assessed the expression of the enzyme activation-induced cytidine deaminase (AID). We observed that both splenic and hepatic B cell blasts and PBs expressed higher amounts of AID than did naive B cells and T cells (Figures S3C–S3E). To further assess SHM, we amplified and sequenced V-region genes from the DNA of splenic and hepatic PBs sorted by fluorescence-activated cell sorting (FACS). The mutation rate was 1% for PBs from spleen and 1.5% for PBs from liver (Figures 3G and 3H). However, approximately 50% of V-gene sequences

in about 1/2 of them. The finding of intracloal diversity among small groups of isolated cells demonstrates ongoing mutation at that site (Jacob et al., 1991; William et al., 2002; Di Niro et al., 2015). Of 11 microdissections from spleen, 6 had clones with sequences that were mutated from the closest germline (GL) Vh gene (Table S1). Of 10 microdissections from the liver, 7 had sequences that were mutated from the closest GL Vh gene (Table S1). These clonally related sequences could be assembled into 4 clonal lineage trees from spleen (Figure 3I; Figure S3F) and 4 clonal lineage trees from liver (Figure 3J; Figure S3G). The finding in multiple cases at each site that there were cells that shared mutations (i.e., the clones had trunks) and also differed by other mutations (i.e., the clones had branches) provides evidence that SHM occurred locally in spleen and in liver parenchyma.

Repertoire Characteristics of the Acute B Cell Response in Spleen and Liver

Next, to more deeply investigate the extent of SHM and the magnitude of overlap of the responding B cell repertoire in different B cell populations at both sites, we performed HTS of

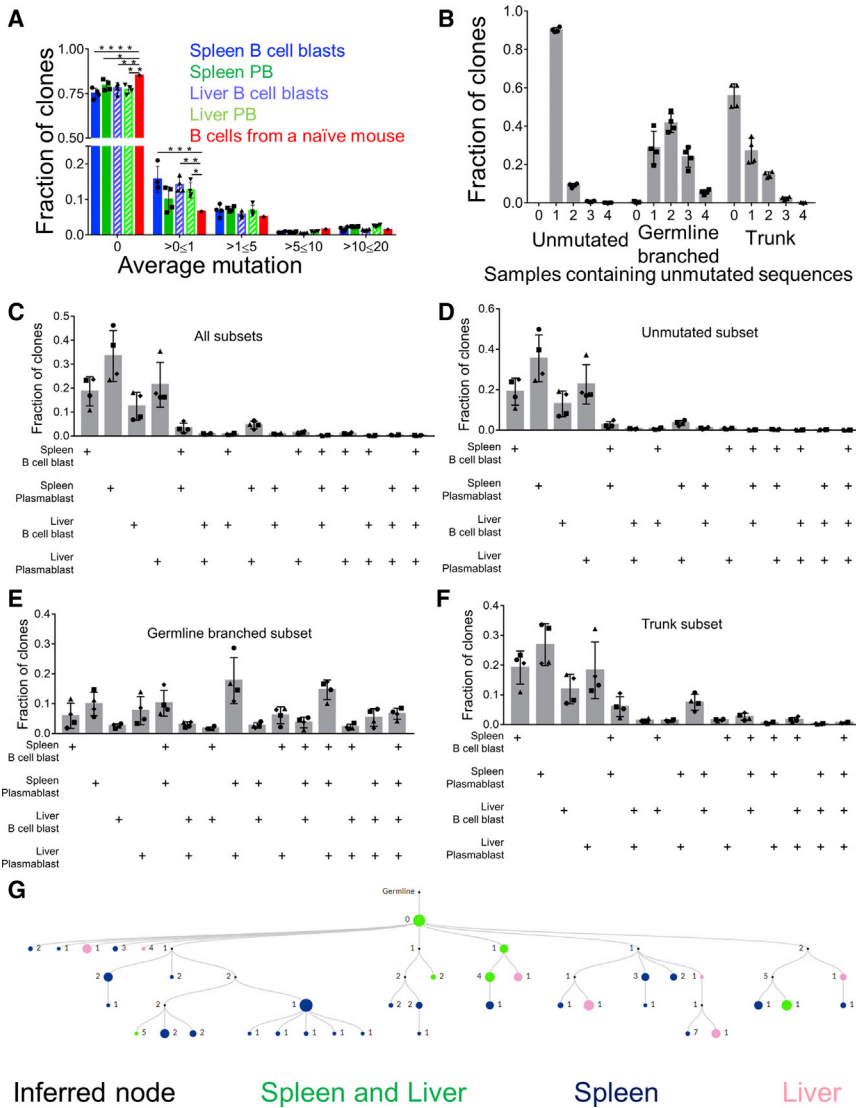


Figure 4. SHM in Spleen and Liver B Cell Blasts and PBs

(A) Mutation distribution in populations of splenic and hepatic B cell blasts and PBs.

(B) Fraction of unmutated, GL-branched, and trunk clones found in any of the 4 populations of hepatic and splenic B cell blasts and PBs.

(C–F) Fraction of clones shared within populations of splenic and hepatic B cell blasts and PBs of all clones (C), unmutated clones (D), GL-branched clones (E), and trunk clones (F).

(G) An example of a multi-tiered clonal lineage found in both spleen and liver.

Nodes found in both organs are green, nodes found in spleen only are blue, nodes found in liver only are pink, and inferred nodes are black. Node size is proportional to the number of sequences. * $p < 0.05$, ** $p < 0.01$, *** $p < 0.001$, **** $p < 0.0001$.

Statistics for (A) were done by 2-way ANOVA. See Figure S4.

clonal-lineage characteristics into 3 groups that might reflect different origins or patterns of clonal expansion: unmutated, GL branched (mutated clones that do not have a common shared mutation), and trunk (clones that have a common shared mutation and bifurcate further). Although the total number of unmutated clones was the greatest (at ~75%, Figure 4A), GL-branched clones were substantially larger in terms of both clone size and “instances” (defined as total number of unique sequences), whereas trunk clones were intermediate (Figures S4A and S4B). Hence, although the number of unmutated clones was greater, those that did mutate had expanded considerably

the heavy-chain VDJ (variable, diversity, and joining gene segment) mRNA, as described previously (Di Niro et al., 2015). We FACS sorted splenic and hepatic B cell blasts and PBs on day 13 after infection and created libraries with V-region sequences of these 4 populations. HTS analysis was done as previously described (Rosenfeld et al., 2018; Sheneman et al., 2006). We assembled the clones by using ImmuneDB (see STAR Methods), but to avoid spurious results, we included them in this analysis only if they had 1–4 non-templated complementarity-determining region 3 (CDR3) residues (as measured from the first non-GL-encoded nucleotide) or had at least 4 common V-gene mutations across all sequences. We found that about 75% of the clones within the 4 populations were unmutated (Figure 4A), suggesting that *Ehrlichia* infection induced SHM in only a subset of B cells, which is consistent with our sequencing and microdissection results (Figures 3G–3J). Overall, 10%–15% of the clones had an average mutation value of >0 and ≤ 1 , and 5%–10% of the clones had an average of 1–5 mutations (Figure 4A). To gain insight into how clones grew and migrated, we categorized the clones according to their

in terms of numbers of sequences and thus presumably in terms of numbers of cells.

Within each category we then assessed the extent of the sharing of clones among the 4 populations that were sequenced. Among unmutated clones, the vast majority (~90%) were found in only 1 population, and only 10% were found in as many as 2 populations (Figure 4B). However, the GL-branched clones demonstrated extensive spread among the different populations: 40% of clones were found in 2 populations, ~25% clones were found in 3 populations, and ~5% were shared among all 4 populations (Figure 4B). In the case of the trunk clones, we found that about 20% of the clones were shared between 2 popula-

tions (Figure 4B). To determine patterns of migration and differentiation, we assessed the fraction of clones that overlapped among all the populations; this was a minimal estimate as a result of limited sampling. Overall, splenic and hepatic PBs demonstrated the most overlap (~5%) (Figure 4C). Upon breaking down the clones on the basis of their unique clonal-lineage categories defined above, we found that splenic and hepatic PB populations

exhibited the most overlap, which amounted to ~20% of the GL-branched subset and 5% of the trunk subset (Figures 4D–4F). The GL-branched category demonstrated the most overlap, wherein 15% of the clones were shared among splenic B cell blasts and PBs along with hepatic PBs, and 5% of the clones were shared by all 4 populations (Figure 4E). Analysis of the selection pressure on the B cell clones revealed that the responding GL-branched clones exhibited a greater degree of selection pressure than did trunk clones (Figures S4C–S4F). Overall, these data demonstrate that *Ehrlichia* infection induced SHM in a subset of responding B cells and that within the mutated clones, there was both differentiation and spreading.

These conclusions are further supported by genealogies of representative larger expanded clones that were found in both spleen and liver (Figure 4G; Figures S4G–S4I). In Figures 4G, S4G, and S4I, we show that the clones depicted had a GL sequence that was found in both organs; however, the clone further diversified by accumulating additional mutations that demarcated nodes and branches that were found only in spleen or liver. As shown in Figure S4H, the GL sequence was found only in liver, but other nodes of the clone overlapped between the spleen and liver, and a branch was found to be present only in spleen. These data are most consistent with bidirectional spreading of B cell clones along with continued local mutation and expansion after dissemination.

Memory-like T-bet⁺ B Cells Persist in Spleen and Liver after Infection Subsides

Previously, CD19⁺CD80⁺CD11c⁺T-bet⁺ B cells have been shown to persist in spleen for substantial time periods after initial *Ehrlichia* infection (Papillion et al., 2017; Racine et al., 2008; Racine et al., 2010; Winslow et al., 2017; Kenderes et al., 2018). These were interpreted to depend on inflammation or chronic low-level Ag stimulation because *Ehrlichia muris* causes persistent infection. We sought to determine whether generation and maintenance of both splenic and hepatic MBC populations depend on Ag persistence. To eliminate persistent *Ehrlichia* infection, we treated mice with doxycycline 4 weeks after infection and then examined the MBC responses in spleen and liver between weeks 6 and 12 after infection. We refer to these mice as “memory mice.” We gated on MBCs by using a commonly used marker that includes classical MBC markers, such as CD73 (Anderson et al., 2007), along with T-bet expression (Figure 5A). We found a higher number of MBCs in both spleen and liver of the memory mice than in their naive counterparts (Figures 5A–5C). In both spleen and liver, these cells expressed the classical MBC markers CD80 and PD-L2 in a unimodal fashion (Figure 5D and 5E), whereas a distinct subpopulation of the CD73⁺ T-bet⁺ cells expressed the ABC markers CD11b and CD11c (Figures 5F and 5G). Moreover, these MBCs were quiescent such that few expressed Ki67 (Figure 5H). IgM was expressed by most of the MBCs; the fraction lacking IgM was more predominant in liver (Figure 5I). These findings revealed that CD11b and CD11c, which up to now have been used to identify ABC-type MBCs (Winslow et al., 2017), identify only a fraction—in fact less than half—of all T-bet⁺-elicited MBCs, raising the question of whether there is additional heterogeneity among T-bet-expressing MBCs.

To rule out any contamination from blood-derived MBCs that were not removed from liver by perfusion, we employed an approach that involved the labeling of all circulating B cells via an intravenous injection of CD19-PE. We harvested spleen, blood, and liver 3 min after the injection. Although all the B cells in the blood became labeled, given the short window of time and because of the large size and molecular weight of the fluorophore phycoerythrin (PE), the Ab should not be able to reach the liver parenchyma to a substantial extent. So, any liver-localized MBCs should be CD19-PE^{lo} or CD19-PE⁻. In practice, during tissue processing, tissue-localized cells encounter CD19-PE released from the substantial vascular compartment of liver (which is un-perfused) and thereby become stained, albeit to a substantially lower level. After processing, we further stained the cells with anti-CD19 in a different color (BUV395). In liver, a clear population of cells was much more dimly stained for CD19-PE (~5× dimmer) than for CD19-BUV395 but more brightly stained for CD19-BUV395 than for CD19-PE (Figures S5A and S5B). No such population existed in the blood (Figures S5A and S5B). As expected, spleen had mostly CD19-PE^{lo} cells given that follicular B cells are not directly accessible to blood and were not quickly stained by an Ab (Figures S5A and S5B). About 10% of liver MBCs in un-perfused liver were weakly stained for CD19-PE and brightly stained for CD19-BUV395. Moreover, the number of these cells (i.e., their frequency multiplied by the total cells recovered) was comparable to the number of MBCs that we observed in liver after perfusion (Figure S5C; Figure 5C). These data provide support for the interpretation that a tissue-localized MBC population was observed as persistent after perfusion of liver. The other ~90% of cells that stained brightly with anti-CD19-PE within 3 min in un-perfused liver were presumably in intravascular spaces, such as sinusoids, and these would very largely be washed away by perfusion. Moreover, by histology, we found CD19- and CD11c-expressing MBCs in liver parenchyma of immune mice (Figure S5D). Upon comparison to livers from naive mice, we observed more CD19⁺CD11c⁺ cells per field in the immune mouse livers (Figures S5E and S5F). When taken together, these data suggest that a liver-localized MBC population was induced by *E. muris* infection.

Repertoire and Phenotypic Characteristics of the MBC Response in Spleen and Liver

The validation of CD73 as a marker for T-bet⁺ MBCs in this setting allowed us to FACS sort CD73⁺ hepatic and splenic MBCs from memory mice and perform V-region HTS to assess both SHM and clonal sharing among sites and subsets. As seen from the fraction of clones that were unmutated (Figure 6A), 60% of IgM MBC clones and 80% of IgG MBC clones were mutated in both organs. Overall, IgG clones harbored more mutations than did IgM clones, and 40% of splenic IgG clones and 20% of hepatic IgG clones had an average of 5–20 mutations (Figure 6A). A substantial fraction of clones had 1–5 mutations per sequence, which is comparable to levels seen in MBCs after primary responses to model Ags in GCs (Kaji et al., 2012; Anderson et al., 2007). In addition, these data establish that the MBC compartment localized in liver was mutated similarly to that in spleen. Approximately 90% of the clones were found only in spleen, about 5% were found only in liver, and 5% were shared between spleen and liver (Figures 6B and 6C). The GL-branched

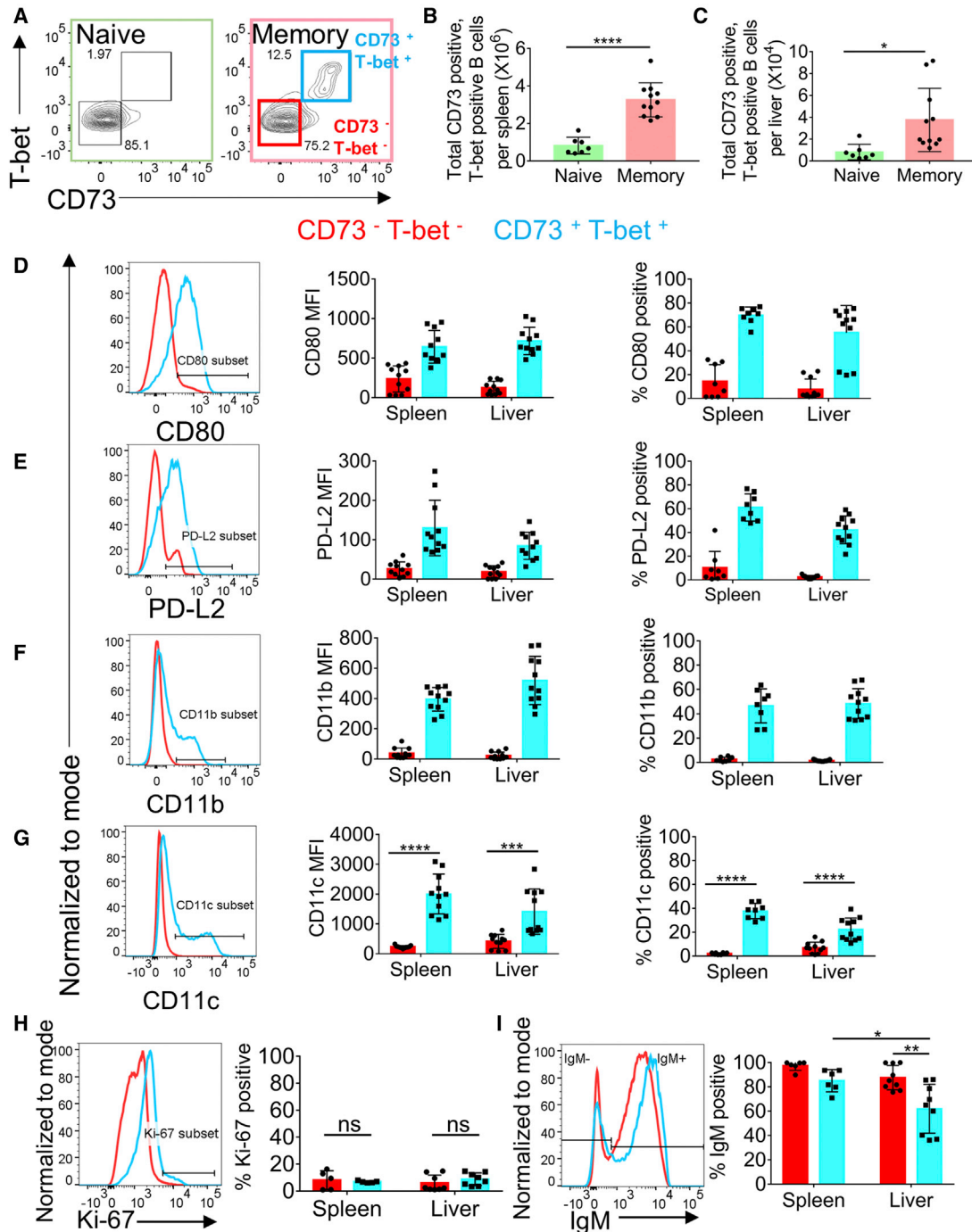
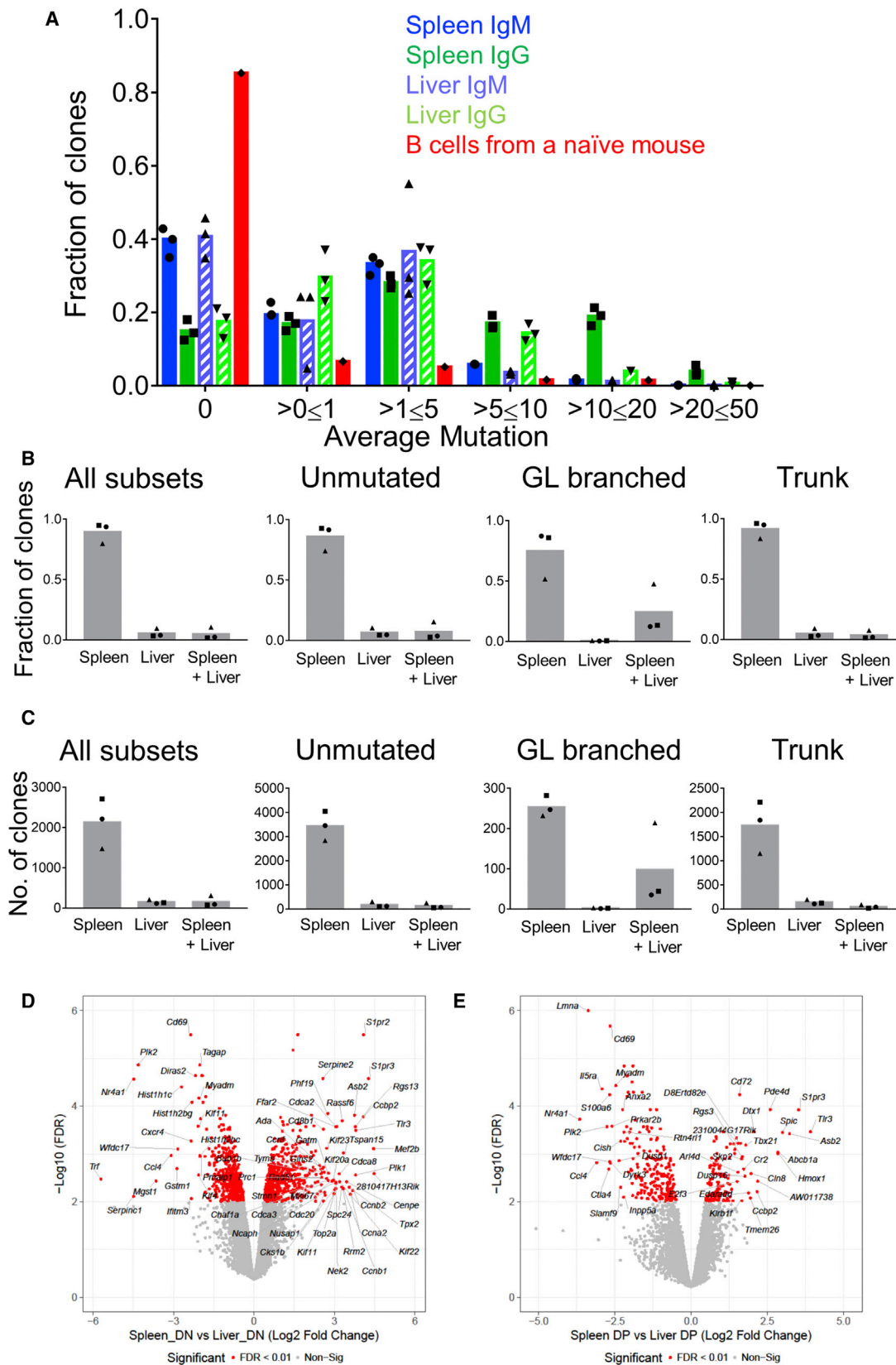


Figure 5. Memory-like T-bet⁺ B Cells Persist in Spleen and Liver after Infection Clearance

(A) Gating strategy for CD73⁺ and T-bet⁺ B cells in spleen and liver of naive and memory mice.
 (B and C) CD73⁺ and T-bet⁺ B cells in spleen (B) and liver (C) harvested after perfusion with phosphate-buffered saline (PBS) of naive and memory mice.
 (D–G) Histogram, mean fluorescence intensity, and percentage of cells positive for CD80 (D), PD-L2 (E), CD11b (F), and CD11c (G) in CD73⁻ and T-bet⁻ cells and CD73⁺ and T-bet⁺ B cells in spleen and liver of memory mice.
 (H and I) Histogram and percentage of Ki-67⁺ cells (H) and histogram and percentage of IgM⁺ cells (I) in CD73⁻ and T-bet⁻ cells and CD73⁺ and T-bet⁺ B cells in spleen and liver of memory mice.
 Data are representative of at least 2 independent experiments, and in (B)–(H), data are represented as mean plus SD of groups of at least 2 mice. *p < 0.05, **p < 0.01, ***p < 0.001, ****p < 0.0001. Statistics for (B), (C), and (I) were done by t test, and statistics for (G) were done by 2-way ANOVA. See Figure S5.



(legend on next page)

category had the most clones shared between spleen and liver, indicative of the fact that this category includes clones with more mutation and expansion but is a smaller category overall in terms of numbers of clones (Figures 6B and 6C). A major reason for the relative lack of overlap of clones in spleen and liver could be the much larger size of the spleen MBC pool and differences in sampling depth. Alternatively, it is possible that only a few splenic MBCs engrafted the liver and/or the majority of liver-derived MBCs engrafted the splenic MBC compartment. Analysis of clonal trees from large clones did reveal trees that were consistent with both migration after differentiation and extensive local production of diversified MBC clonal populations (Figure S6).

To phenotypically characterize the splenic and hepatic MBCs, we performed RNA-sequencing (RNA-seq) analysis of CD11b⁺CD11c⁻ (DN) and CD11b⁺CD11c⁺ (DP) MBCs on FACS-sorted populations from memory mice (Figure S7A). We found 730 genes that were differentially and significantly expressed (false-discovery rate < 0.01, 2-fold change) in the splenic and hepatic MBC populations (Figure S7B; Table S2). Gene clusters marked with navy blue, red, and dark red were significantly and differentially expressed in the DN subsets compared with the DP subsets regardless of the site of origin (Figure S7B). Gene clusters marked with yellow, purple, pink, turquoise blue, and light pink were significantly and differentially expressed in liver MBCs compared with the splenic counterparts (Figure S7B). We found several genes that were differentially and significantly expressed in spleen DN and DP subsets in comparison with their liver counterparts (Figures 6D and 6E). Liver MBC subsets both expressed CD69, whereas splenic MBC subsets did not (Figures 6D and 6E), consistent with the expression patterns of bona fide T resident memory cells (Sathaliyawala et al., 2013). We verified the CD69 expression on the liver MBC subsets during acute response (day 10 after infection) by FC (Figures S7C and S7D). Together, these data demonstrate that although shared genes were expressed in MBC subsets regardless of their tissue localization, several genes were unique to the subset and site of origin. This suggests that the local tissue microenvironment might be shaping the MBC differently in spleen and liver, much as it does for T cells and macrophages (Kumar et al., 2017; Lavin et al., 2014).

We performed gene-set enrichment analysis (GSEA) in comparison to a published dataset from CD11c-expressing splenic B cells that were presumptive MBCs and isolated 30 days after *Ehrlichia* infection (Winslow et al., 2017). GSEA revealed that genes found in that database were enriched in transcriptomes of splenic and hepatic DP MBCs compared with DN MBCs (Figures S7E and S7F). This suggests that our data are consistent with the previously published dataset with reference to *Ehrlichia* infection. We further performed differential analysis of splenic and liver memory subsets with respect to naive B cells from a previously published study (Barnett et al., 2016) (see STAR Methods for inter-study normalization details). Using a set of genes that have higher expression in nitrophenyl-hapten-induced MBCs than in naive B cells (data not

shown), we found that splenic DN, splenic DP, and hepatic DP MBC subsets had an enrichment of memory genes, and hepatic DN MBC subsets had a similar trend (Figures S7G–S7J). These data suggest that *Ehrlichia*-induced splenic DP and DN MBC subsets, along with hepatic DP MBC subsets, express genes that are characteristically expressed by classical, GC-induced MBCs.

T-bet⁺ B Cells Dominantly Repopulate the Splenic MZ after Infection

During the acute phase of *Ehrlichia* infection, the histologic MZ architecture is disrupted, resulting in loss of CD169⁺ metallophilic macrophages that demarcate the MZ (data not shown). FC showed that CD23^{lo}CD21⁺ MZ-phenotype B cells were also absent (Figure 7A). At a memory time point, the histologic MZ was largely regenerated with a border of CD169⁺ cells, albeit somewhat less organized than in a naive animal (Figures 7B and 7C). Nonetheless, at this memory time point, very few of the CD23^{lo}CD21⁺ MZ-phenotype cells that had repopulated this compartment were T-bet⁻, unlike in the naive mouse, in which essentially all MZ-phenotype B cells lacked T-bet expression (Figures 7D and 7E). On average there were 2.3-fold more T-bet⁺ than T-bet⁻ MZ B cells in the memory mice (Figures 7F and 7G). Histologically, in memory mice, T-bet⁺ B cells were found abundantly in the MZ region and were also scattered in the follicular (FO) region (Figure 7C). A prior report had identified CD11c⁺ B cells in or near the MZ at day 63 after infection (Yates et al., 2013), although, as noted earlier, CD11c would only pick up <40% of total T-bet⁺ MBCs. Generally, ABCs are thought to lack the expression of B cell subset markers CD21 (high on MZ B cells) and CD23 (high on FO B cells) (Rubtsova et al., 2015; Rubtsova et al., 2017; Hao et al., 2011). However, a large fraction of the T-bet⁺ MBCs formed in this setting after *Ehrlichia* infection were of a MZ phenotype with strong expression of CD21; in addition, some had an ABC (CD21⁻CD23⁻) or FO phenotype.

To assess whether the FO, MZ, and ABC MBC subsets retain their phenotype and preferentially lodge to those sites upon transfer, we used FACS to purify FO, MZ, and ABC CD45.2 MBCs by using the expression of CD21 and CD23. We labeled the MBC subsets with carboxyfluorescein succinimidyl ester (CFSE) and transferred them into a naive *B18^{+/-}V α 8R^{+/-}CD45.1/2* mouse. We harvested the spleens of the host 42 h after the transfer to assess homing of the MBC subsets. According to histologic analysis, >50% of FO MBCs preferentially populated the follicle, >70% of MZ MBCs populated the MZ area, and the ABCs populated all the zones (Figures 7H and 7I). These data suggest that the MBC subsets could rehome to the compartment that they originated in and that their localization is a relatively stable characteristic.

DISCUSSION

Here, we found that liver is a generative site of B cell responses during local infection of the liver. Local B cell responses in

Figure 6. Repertoire and Phenotypic Characteristics of the MBC Population in Spleen and Liver

(A) Mutation distribution of the MBC population in spleen and liver from memory mice and B cells from a naive mouse. (B and C) The distribution of clones with respect to whether they were found in spleen only, liver only, or both liver and spleen for the different types of MBC clones, as analyzed by fraction of clones (B) and number of clones (C). (D and E) Volcano plots demonstrating highly expressed genes in spleen and liver DN (D) and DP (E) MBC subsets. See Figures S6 and S7 and Table S2.

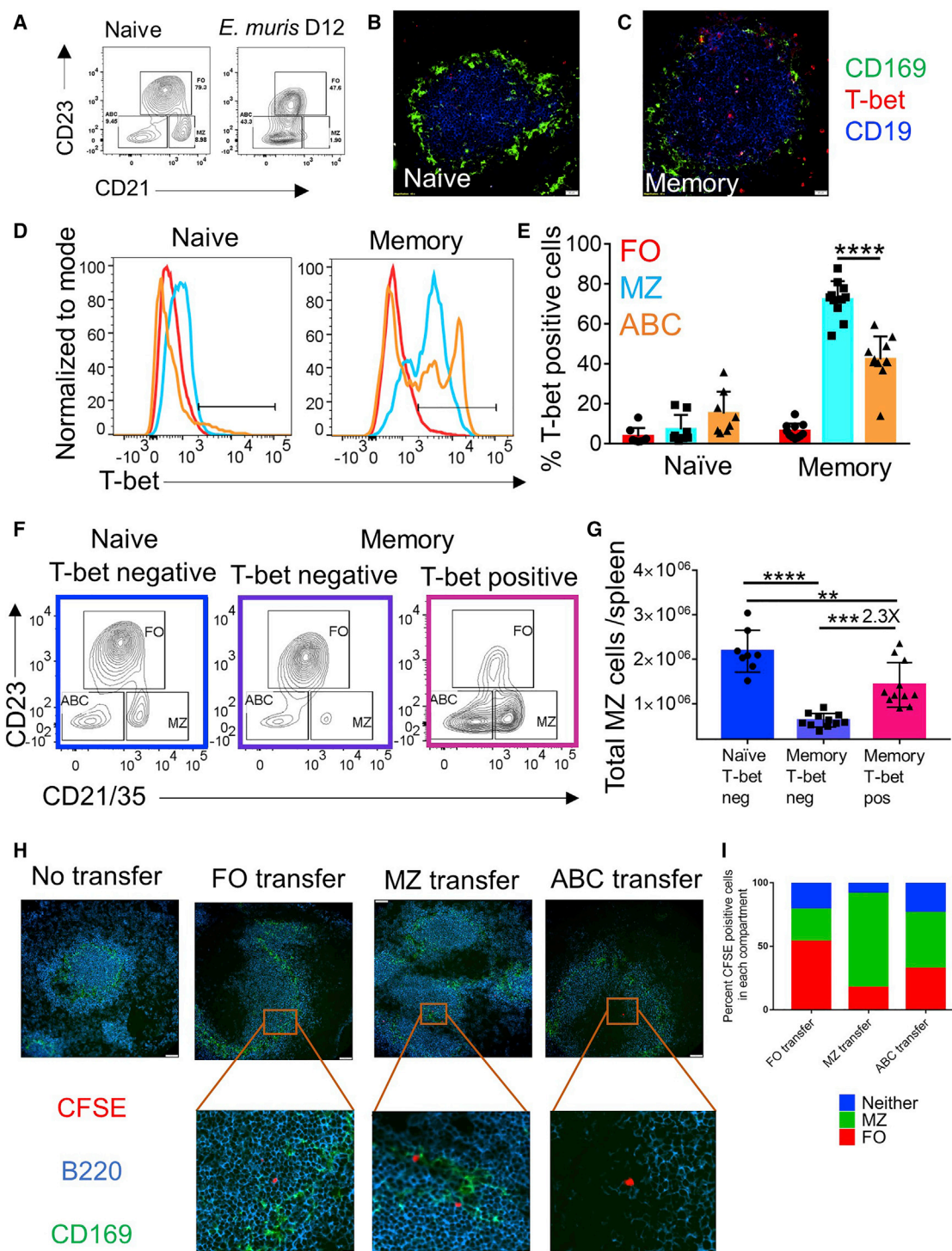


Figure 7. After Infection Resolves, T-bet⁺ MBCs Dominate the MZ of Spleen

(A) B cell subset gating on CD19⁺ B cells in naive or D12 after *E. muris* infection.

(B and C) CD169 (green), T-bet (red), and CD19 (blue) staining in naive (B) and memory spleens (C) at 40 \times magnification. Scale bars represent 20 μ m.

(D and E) Histogram (D) and percentage (E) of T-bet⁺ B cells in naive and memory mice.

(F) B cell subset gating on naive and memory T-bet⁺ B cells.

(G) Quantification of T-bet⁺ MZ B cells in naive and memory mice.

(H) 20 \times images of CFSE-labeled CD19⁺CD73⁺CD45.2/2 splenic MBC populations sorted as CD23⁺CD21⁻ (FO), CD21⁺CD23⁻ (MZ), and CD21⁻CD23⁻ (ABC) and transferred into CD45.1/2 mice are shown 42 h after transfer. Scale bars represent 50 μ m (top) and 10 μ m (bottom).

(legend continued on next page)

non-lymphoid organs have been reported in several other contexts. Influenza infection yields lung responses that involve generation of tertiary lymphoid tissue (Moyron-Quiroz et al., 2004). Local production of immunoglobulin A (IgA) AFCs in the lamina propria (Fagarasan et al., 2001) is most likely driven by commensal flora (Kunisawa et al., 2013; Fagarasan et al., 2002). However, unlike lung and gut, liver has no direct mucosal interface with the environment.

Hepatitis infection in humans also can generate B cell infiltration, including tertiary lymphoid tissue and local GC formation (Farci et al., 2010; Murakami et al., 1999; Racanelli et al., 2001; Sansonno et al., 2004). In contrast, hepatic *E. muris* infection did not induce tertiary lymphoid tissue or GCs, yet SHM and class switch were induced in a fraction of responding cells in liver. Intrahepatic responses to *E. muris* involved both portal triads and foci that were within the parenchyma itself. Thus, under circumstances of infection, robust and mature local B cell responses can ensue directly within parenchymal tissue.

The advantages of mounting local B cell responses are several. Some pathogens might not infect or spread well to lymphoid tissue. Pathogens such as *E. muris* and Plasmodium might clear systemically but persist in liver as low-level infections (Dumler et al., 1993; Mueller et al., 2009; Crocquet-Valdes et al., 2011; Thirumalapura et al., 2009; Thirumalapura et al., 2008). Therefore, if local B cell responses were not possible, then there might be little if any Ab produced against such pathogens. Intraparenchymal T cell responses and infiltration are more commonly seen; local B cell responses might optimize these because they would allow for enhanced Ag presentation to T cells. In addition, B cells produce substantial amounts of inflammatory cytokines, such as IL-6 and TNF- α , which could stimulate other arms of the immune system and be directly protective in a local manner.

HTS of V regions revealed extensive cross-site clonal mixing. Although limited sampling depth led to a general underestimation of the extent of clonal size, diversification, and cross seeding of tissues, it is reasonable to assume that not all clones disseminated. Overall, mutation was observed in only about 25% of clones, and these clones, which we termed “GL branched,” tended to be found in multiple sites and in both PBs and B cell blast compartments. These clones were evidently much larger than those in either the unmutated or trunk subset. It is not clear what controls whether clones initiate SHM and expand to a greater extent; it could be affinity-driven and/or dependent on proximity to sites of proliferating bacteria and thereby the degree of persistent Ag-stimulation as well as T cell help.

Patterns of distribution of clone members were most consistent with bidirectional interchange of both PBs and B cell blasts in clones that were expanding and undergoing SHM. Regardless of how such clones evolved, their disseminating nature illuminates an immune system feature that would anticipate pathogen dissemination by enabling actively responding B cell clones to populate sites distant from where they received their initial stimulus and thus create a more comprehensive and adaptive

immune response. Compared with responding B cells at early time points after infection, MBC clones had more V-region mutation. This suggests that either most MBCs were formed at later time points in the response, after more mutations accumulated, or the more expanded clones that had more mutation were more likely to spawn longer-lived MBCs.

At steady state, expanded B cell clones are also disseminated in normal humans (Meng et al., 2017). Cerutti and colleagues identified an IgM MBC subset, disseminated throughout human gut, that does not share clonal origin with most peripheral MBCs but is the precursor of local IgM and IgA production (Magri et al., 2017). These MBCs are most likely driven by gut commensals, but their precise site of origin remains unclear. In analogous elegant studies, Lindner et al. found dispersed clones of MBCs in multiple Peyer’s patches, though they did not examine lamina propria; these MBCs migrate to spleen, and they are clonally related to mammary gland IgA plasma cells (Lindner et al., 2012). In these settings, the inductive phase was considered to occur in secondary lymphoid tissue and lead to the subsequent spread of both MBC and plasma cells.

We conclude that many of the B cells that were detected in liver at memory time points were MBCs; it is unlikely that they were blood passenger B cells that remained despite our perfusion of the liver prior to harvest. Their memory characteristics, including isotype switch in a fraction, V-region mutation, and particularly expression of T-bet, CD73, and CD80, are all unlike B cells found in blood. Intravenous injection of anti-CD19-PE also demonstrated the presence of a liver-localized MBC population that was resistant to rapid labeling. Because we have not directly studied their migration, we prefer to call these cells “tissue-localized” MBCs rather than “tissue-resident” to reflect that they were neither in lymphoid structures nor intravascular. The length of residence of the MBCs we identified remains to be determined. Although tissue MBCs are relatively less studied than their T cell counterparts, prior work has identified such cells in gut at steady state in both mice and humans, and they can be induced by influenza infection or oral immunization in mice (Onodera et al., 2012; Bemark et al., 2016).

The presence of MBCs localized in liver after the clearance of the infection is distinctive in that, unlike lung and gut, liver is not a mucosal barrier site. However, MBC populations are clearly identified during *chronic* liver disease, such as chronic hepatitis and autoimmunity, in humans. In these cases, continuous immune stimulation is most likely responsible for the development and maintenance of such populations. By analogy, MBCs in liver after *E. muris* infection might have been formed from prior local acute responses and/or might have migrated from splenic populations, as exemplified by clones that were both liver specific and found in both spleen and liver. The functional implications of liver-localized MBCs for subsequent infection and protection are unclear, but it is tempting to speculate that they can provide protection for certain types of local reinfection, as is proposed for resident memory T cells (Kumar et al., 2017) and certain

(I) From the recipient mice as in (H), 67 CFSE-labeled cells from the FO transfer group were counted over 42 images, 108 CFSE-labeled cells from the MZ transfer group were counted over 21 images, and 105-CFSE labeled cells from the ABC transfer group were counted over 44 images.

Percentages of the CFSE⁺ transferred MBC subsets found in FO, MZ, or neither of those locations are presented in the bar graphs. Data are representative of at least 2 independent experiments with groups of at least 2 mice. In (E) and (G), data are represented as mean plus SD, and statistics were done by 2-way ANOVA. * $p < 0.05$, ** $p < 0.01$, *** $p < 0.001$, **** $p < 0.0001$.

types of tissue-localized MBCs (Onodera et al., 2012; Bemark et al., 2016).

Our findings also have implications for understanding T-bet⁺ cells in terms of their origins, identities, locations, and functions. In agreement with others (Kenderes et al., 2018; Winslow et al., 2017), we confirmed that these cells were indeed MBCs and largely non-proliferative. Although previous reports in the context of *E. muris* have relied on CD11c expression as a surrogate marker, we found that a full 50% of T-bet⁺ MBCs did not express CD11c or CD11b. Conversely, there were also many that *did* express CD21 and CD23, although the canonical ABCs are described as not expressing those markers (Rubtsova et al., 2015; Rubtsova et al., 2017). This basic immunophenotyping revealed considerable heterogeneity among the *E. muris*-induced T-bet⁺ MBCs. Moreover, RNA-seq analysis demonstrated not only that certain shared genes were expressed in MBC subsets regardless of their tissue location but also a substantial number of genes unique to the particular subset and site of origin. This suggests that the local tissue microenvironment might shape the MBCs differently in spleen and in liver.

Finally, in the course of tracking the B cell response to *E. muris*, we unexpectedly found that infection caused a wholesale remodeling of the splenic MZ. MZ disruption, as part of more pervasive splenic-architecture disruption, has been previously reported in the context of multiple infections, such as lymphocytic choriomeningitis virus, salmonella, and malaria (Rosche et al., 2015; Müller et al., 2002; Urban et al., 2005). However, after *E. muris* infection, during the eventual reorganization, the MZ was repopulated by MBCs induced by infection rather than by the more typical primary MZ B cells. Hence, the repertoire and presumably the functional capacity of the MZ B cell compartment were markedly reprogrammed such that ~70% of MZ-phenotype B cells expressed T-bet after infection, whereas a negligible proportion was expressed prior to infection. This major alteration lasted for at least 8 weeks after infection and, we assume, for much longer. It is unclear why T-bet⁺ B cells, rather than naive MZ B cells, preferentially repopulate the MZ. This type of mechanism might explain the observed presence of mutated IgM MBCs in the MZ of human spleens (Weller et al., 2004). We further propose that, given the importance of MZ B cells in responding acutely to various infections (Martin et al., 2001; Bankoti et al., 2012), the remodeling of the MZ by *E. muris*, and potentially other similar primary infections, could be a mechanism by which a significant initial infection could alter or impair the response to subsequent infection.

STAR★METHODS

Detailed methods are provided in the online version of this paper and include the following:

- KEY RESOURCES TABLE
- LEAD CONTACT AND MATERIALS AVAILABILITY
- EXPERIMENTAL MODEL AND SUBJECT DETAILS
- METHOD DETAILS
 - Infection and Treatment Procedures
 - ELISpot Assays
 - Flow Cytometry
 - Immunofluorescence imaging

- V region sequencing
- Cell Sorting and RNA preparation
- HTS library preparation and analysis
- RNA seq analysis
- QUANTIFICATION AND STATISTICAL ANALYSIS
- DATA AND CODE AVAILABILITY

SUPPLEMENTAL INFORMATION

Supplemental Information can be found online at <https://doi.org/10.1016/j.immuni.2019.10.004>.

ACKNOWLEDGMENTS

We thank Dr. David Walker at the University of Texas Medical Branch for providing *E. muris* Ags Omp12 and Omp19. We thank the Histology Core at Magee Research Institute for laser micro-dissections. We are thankful to Laura Center and Rachel Green for helping with the experiments. This work was funded by NIH grants NIH-1R01AI105018 and NIH-2R01AI043603. A.M.R. was supported by NIH grant P01-AI106697.

AUTHOR CONTRIBUTIONS

N.T. designed and performed the experiments, analyzed the data, and wrote the manuscript. F.W., S.J., and M.K. performed the experiments and analyzed the data. A.R.K. and C.C. prepared the HTS libraries. A.M.R. analyzed the HTS data. S.S. and M.C. analyzed the RNA-seq data. F.V., U.H., and N.I. supervised the experiments. M.J.S. designed the experiments, analyzed the data, supervised the experiments, and wrote the manuscript.

DECLARATION OF INTERESTS

The authors declare no competing interests.

Received: January 27, 2019
 Revised: July 24, 2019
 Accepted: October 15, 2019
 Published: November 12, 2019

REFERENCES

- Anderson, B.E., Dawson, J.E., Jones, D.C., and Wilson, K.H. (1991). Ehrlichia chaffeensis, a new species associated with human ehrlichiosis. *J. Clin. Microbiol.* 29, 2838–2842.
- Anderson, S.M., Tomayko, M.M., Ahuja, A., Haberman, A.M., and Shlomchik, M.J. (2007). New markers for murine memory B cells that define mutated and unmutated subsets. *J. Exp. Med.* 204, 2103–2114.
- Bankoti, R., Gupta, K., Levchenko, A., and Stäger, S. (2012). Marginal zone B cells regulate antigen-specific T cell responses during infection. *J. Immunol.* 188, 3961–3971.
- Barnett, B.E., Staupe, R.P., Odorizzi, P.M., Palko, O., Tomov, V.T., Mahan, A.E., Gunn, B., Chen, D., Paley, M.A., Alter, G., et al. (2016). Cutting Edge: B Cell-Intrinsic T-bet Expression Is Required To Control Chronic Viral Infection. *J. Immunol.* 197, 1017–1022.
- Barry, W.T., Nobel, A.B., and Wright, F.A. (2008). A statistical framework for testing functional categories in microarray data. *Annals of Applied Statistics* 2, 286–315.
- Bemark, M., Hazanov, H., Strömberg, A., Komban, R., Holmqvist, J., Köster, S., Mattsson, J., Sikora, P., Mehr, R., and Lycke, N.Y. (2016). Limited clonal relatedness between gut IgA plasma cells and memory B cells after oral immunization. *Nat. Commun.* 7, 12698.
- Coro, E.S., Chang, W.L., and Baumgarth, N. (2006). Type I IFN receptor signals directly stimulate local B cells early following influenza virus infection. *J. Immunol.* 176, 4343–4351.
- Crocquet-Valdes, P.A., Thirumalapura, N.R., Ismail, N., Yu, X., Saito, T.B., Stevenson, H.L., Pietzsch, C.A., Thomas, S., and Walker, D.H. (2011).

- Immunization with Ehrlichia P28 outer membrane proteins confers protection in a mouse model of ehrlichiosis. *Clin. Vaccine Immunol.* 18, 2018–2025.
- Cunningham, A.F., Gaspal, F., Serre, K., Mohr, E., Henderson, I.R., Scott-Tucker, A., Kenny, S.M., Khan, M., Toellner, K.M., Lane, P.J., and MacLennan, I.C. (2007). Salmonella induces a switched antibody response without germinal centers that impedes the extracellular spread of infection. *J. Immunol.* 178, 6200–6207.
- Dawson, J.E., Anderson, B.E., Fishbein, D.B., Sanchez, J.L., Goldsmith, C.S., Wilson, K.H., and Duntley, C.W. (1991). Isolation and characterization of an Ehrlichia sp. from a patient diagnosed with human ehrlichiosis. *J. Clin. Microbiol.* 29, 2741–2745.
- Di Niro, R., Lee, S.J., Vander Heiden, J.A., Elsner, R.A., Trivedi, N., Bannock, J.M., Gupta, N.T., Kleinstein, S.H., Vigneault, F., Gilbert, T.J., et al. (2015). Salmonella Infection Drives Promiscuous B Cell Activation Followed by Extrafollicular Affinity Maturation. *Immunity* 43, 120–131.
- Dobin, A., Davis, C.A., Schlesinger, F., Drenkow, J., Zaleski, C., Jha, S., Batut, P., Chaisson, M., and Gingeras, T.R. (2013). STAR: ultrafast universal RNA-seq aligner. *Bioinformatics* 29, 15–21.
- Dumler, J.S., Sutker, W.L., and Walker, D.H. (1993). Persistent infection with Ehrlichia chaffeensis. *Clin. Infect. Dis.* 17, 903–905.
- Fagarasan, S., Kinoshita, K., Muramatsu, M., Ikuta, K., and Honjo, T. (2001). In situ class switching and differentiation to IgA-producing cells in the gut lamina propria. *Nature* 413, 639–643.
- Fagarasan, S., Muramatsu, M., Suzuki, K., Nagaoka, H., Hiai, H., and Honjo, T. (2002). Critical roles of activation-induced cytidine deaminase in the homeostasis of gut flora. *Science* 298, 1424–1427.
- Farci, P., Diaz, G., Chen, Z., Govindarajan, S., Tice, A., Agulto, L., Pittaluga, S., Boon, D., Yu, C., Engle, R.E., et al. (2010). B cell gene signature with massive intrahepatic production of antibodies to hepatitis B core antigen in hepatitis B virus-associated acute liver failure. *Proc. Natl. Acad. Sci. USA* 107, 8766–8771.
- Habib, S., El Andaloussi, A., Hisham, A., and Ismail, N. (2016). NK Cell-Mediated Regulation of Protective Memory Responses against Intracellular Ehrlichial Pathogens. *PLoS ONE* 11, e0153223.
- Hao, Y., O'Neill, P., Naradikian, M.S., Scholz, J.L., and Cancro, M.P. (2011). A B-cell subset uniquely responsive to innate stimuli accumulates in aged mice. *Blood* 118, 1294–1304.
- Hastey, C.J., Elsner, R.A., Barthold, S.W., and Baumgarth, N. (2012). Delays and diversions mark the development of B cell responses to Borrelia burgdorferi infection. *J. Immunol.* 188, 5612–5622.
- Huerta-Cepas, J., Serra, F., and Bork, P. (2016). ETE 3: Reconstruction, Analysis, and Visualization of Phylogenomic Data. *Mol. Biol. Evol.* 33, 1635–1638.
- Intlekofer, A.M., Banerjee, A., Takemoto, N., Gordon, S.M., Dejong, C.S., Shin, H., Hunter, C.A., Wherry, E.J., Lindsten, T., and Reiner, S.L. (2008). Anomalous type 17 response to viral infection by CD8+ T cells lacking T-bet and eomesodermin. *Science* 321, 408–411.
- Ismail, N., and McBride, J.W. (2017). Tick-Borne Emerging Infections: Ehrlichiosis and Anaplasmosis. *Clin. Lab. Med.* 37, 317–340.
- Ismail, N., Soong, L., McBride, J.W., Valbuena, G., Olano, J.P., Feng, H.M., and Walker, D.H. (2004). Overproduction of TNF- α by CD8+ type 1 cells and down-regulation of IFN- γ production by CD4+ Th1 cells contribute to toxic shock-like syndrome in an animal model of fatal monocytotropic ehrlichiosis. *J. Immunol.* 172, 1786–1800.
- Ismail, N., Bloch, K.C., and McBride, J.W. (2010). Human ehrlichiosis and anaplasmosis. *Clin. Lab. Med.* 30, 261–292.
- Jacob, J., Kelsoe, G., Rajewsky, K., and Weiss, U. (1991). Intracelular generation of antibody mutants in germinal centres. *Nature* 354, 389–392.
- Jegerlehner, A., Maurer, P., Bessa, J., Hinton, H.J., Kopf, M., and Bachmann, M.F. (2007). TLR9 signaling in B cells determines class switch recombination to IgG2a. *J. Immunol.* 178, 2415–2420.
- Kaji, T., Ishige, A., Hikida, M., Taka, J., Hijikata, A., Kubo, M., Nagashima, T., Takahashi, Y., Kurosaki, T., Okada, M., et al. (2012). Distinct cellular pathways select germline-encoded and somatically mutated antibodies into immunological memory. *J. Exp. Med.* 209, 2079–2097.
- Kenderes, K.J., Levack, R.C., Papillion, A.M., Cabrera-Martinez, B., Dishaw, L.M., and Winslow, G.M. (2018). T-Bet+ IgM Memory Cells Generate Multi-lineage Effector B Cells. *Cell Rep* 24, 824–837.
- Khalil, A.M., Cambier, J.C., and Shlomchik, M.J. (2012). B cell receptor signal transduction in the GC is short-circuited by high phosphatase activity. *Science* 336, 1178–1181.
- Kumar, B.V., Ma, W., Miron, M., Granot, T., Guyer, R.S., Carpenter, D.J., Senda, T., Sun, X., Ho, S.H., Lerner, H., et al. (2017). Human Tissue-Resident Memory T Cells Are Defined by Core Transcriptional and Functional Signatures in Lymphoid and Mucosal Sites. *Cell Rep.* 20, 2921–2934.
- Kunisawa, J., Gohda, M., Hashimoto, E., Ishikawa, I., Higuchi, M., Suzuki, Y., Goto, Y., Panea, C., Ivanov, I.I., Sumiya, R., et al. (2013). Microbe-dependent CD11b+ IgA+ plasma cells mediate robust early-phase intestinal IgA responses in mice. *Nat. Commun.* 4, 1772.
- Lavin, Y., Winter, D., Blecher-Gonen, R., David, E., Keren-Shaul, H., Merad, M., Jung, S., and Amit, I. (2014). Tissue-resident macrophage enhancer landscapes are shaped by the local microenvironment. *Cell* 159, 1312–1326.
- Law, C.W., Chen, Y., Shi, W., and Smyth, G.K. (2014). voom: Precision weights unlock linear model analysis tools for RNA-seq read counts. *Genome Biol.* 15, R29.
- Liao, Y., Smyth, G.K., and Shi, W. (2014). featureCounts: an efficient general purpose program for assigning sequence reads to genomic features. *Bioinformatics* 30, 923–930.
- Lindner, C., Wahl, B., Föhse, L., Suerbaum, S., Macpherson, A.J., Prinz, I., and Pabst, O. (2012). Age, microbiota, and T cells shape diverse individual IgA repertoires in the intestine. *J. Exp. Med.* 209, 365–377.
- Magri, G., Comerma, L., Pybus, M., Sintes, J., Lliger, D., Segura-Garzon, D., Bascones, S., Yeste, A., Grasset, E.K., Gutzeit, C., Uzzan, M., et al. (2017). Human Secretory IgM Emerges from Plasma Cells Clonally Related to Gut Memory B Cells and Targets Highly Diverse Commensals. *Immunity* 47, 118–134.
- Martin, F., Oliver, A.M., and Kearney, J.F. (2001). Marginal zone and B1 B cells unite in the early response against T-independent blood-borne particulate antigens. *Immunity* 14, 617–629.
- Meng, W., Zhang, B., Schwartz, G.W., Rosenfeld, A.M., Ren, D., Thome, J.J.C., Carpenter, D.J., Matsuoka, N., Lerner, H., Friedman, A.L., et al. (2017). An atlas of B-cell clonal distribution in the human body. *Nat. Biotechnol.* 35, 879–884.
- Miura, K., and Rikihisa, Y. (2009). Liver transcriptome profiles associated with strain-specific Ehrlichia chaffeensis-induced hepatitis in SCID mice. *Infect. Immun.* 77, 245–254.
- Moir, S., Ho, J., Malaspina, A., Wang, W., DiPoto, A.C., O'Shea, M.A., Roby, G., Kottlilil, S., Arthos, J., Proschian, M.A., et al. (2008). Evidence for HIV-associated B cell exhaustion in a dysfunctional memory B cell compartment in HIV-infected viremic individuals. *J. Exp. Med.* 205, 1797–1805.
- Moyron-Quiroz, J.E., Rangel-Moreno, J., Kusser, K., Hartson, L., Sprague, F., Goodrich, S., Woodland, D.L., Lund, F.E., and Randall, T.D. (2004). Role of inducible bronchus associated lymphoid tissue (iBALT) in respiratory immunity. *Nat. Med.* 10, 927–934.
- Mueller, I., Galinski, M.R., Baird, J.K., Carlton, J.M., Kochar, D.K., Alonso, P.L., and del Portillo, H.A. (2009). Key gaps in the knowledge of Plasmodium vivax, a neglected human malaria parasite. *Lancet Infect. Dis.* 9, 555–566.
- Müller, S., Hunziker, L., Enzler, S., Bühler-Jungo, M., Di Santo, J.P., Zinkernagel, R.M., and Mueller, C. (2002). Role of an intact splenic microarchitecture in early lymphocytic choriomeningitis virus production. *J. Virol.* 76, 2375–2383.
- Murakami, J., Shimizu, Y., Kashii, Y., Kato, T., Minemura, M., Okada, K., Nambu, S., Takahara, T., Higuchi, K., Maeda, Y., et al. (1999). Functional B-cell response in intrahepatic lymphoid follicles in chronic hepatitis C. *Hepatology* 30, 143–150.

- Naradikian, M.S., Hao, Y., and Cancro, M.P. (2016). Age-associated B cells: key mediators of both protective and autoreactive humoral responses. *Immunol. Rev.* **269**, 118–129.
- Olano, J.P., Wen, G., Feng, H.M., McBride, J.W., and Walker, D.H. (2004). Histologic, serologic, and molecular analysis of persistent ehrlichiosis in a murine model. *Am. J. Pathol.* **165**, 997–1006.
- Onodera, T., Takahashi, Y., Yokoi, Y., Ato, M., Kodama, Y., Hachimura, S., Kurosaki, T., and Kobayashi, K. (2012). Memory B cells in the lung participate in protective humoral immune responses to pulmonary influenza virus reinfection. *Proc. Natl. Acad. Sci. USA* **109**, 2485–2490.
- Papillion, A.M., Kenderes, K.J., Yates, J.L., and Winslow, G.M. (2017). Early derivation of IgM memory cells and bone marrow plasmablasts. *PLoS ONE* **12**, e0178853.
- Peng, S.L., Szabo, S.J., and Glimcher, L.H. (2002). T-bet regulates IgG class switching and pathogenic autoantibody production. *Proc. Natl. Acad. Sci. USA* **99**, 5545–5550.
- Racanelli, V., Sansonno, D., Piccoli, C., D'Amore, F.P., Tucci, F.A., and Dammacco, F. (2001). Molecular characterization of B cell clonal expansions in the liver of chronically hepatitis C virus-infected patients. *J. Immunol.* **167**, 21–29.
- Racine, R., Chatterjee, M., and Winslow, G.M. (2008). CD11c expression identifies a population of extrafollicular antigen-specific splenic plasmablasts responsible for CD4 T-independent antibody responses during intracellular bacterial infection. *J. Immunol.* **181**, 1375–1385.
- Racine, R., Jones, D.D., Chatterjee, M., McLaughlin, M., Macnamara, K.C., and Winslow, G.M. (2010). Impaired germinal center responses and suppression of local IgG production during intracellular bacterial infection. *J. Immunol.* **184**, 5085–5093.
- Ritchie, M.E., Phipson, B., Wu, D., Hu, Y., Law, C.W., Shi, W., and Smyth, G.K. (2015). limma powers differential expression analyses for RNA-sequencing and microarray studies. *Nucleic Acids Res.* **43**, e47.
- Rosche, K.L., Aljasham, A.T., Kipfer, J.N., Piatkowski, B.T., and Konjufca, V. (2015). Infection with *Salmonella enterica* Serovar Typhimurium Leads to Increased Proportions of F4/80+ Red Pulp Macrophages and Decreased Proportions of B and T Lymphocytes in the Spleen. *PLoS ONE* **10**, e0130092.
- Rosenfeld, A.M., Meng, W., Luning Prak, E.T., and Hershberg, U. (2018). ImmuneDB, a Novel Tool for the Analysis, Storage, and Dissemination of Immune Repertoire Sequencing Data. *Front. Immunol.* **9**, 2107.
- Rubtsov, A.V., Rubtsova, K., Fischer, A., Meehan, R.T., Gillis, J.Z., Kappler, J.W., and Marrack, P. (2011). Toll-like receptor 7 (TLR7)-driven accumulation of a novel CD11c⁺ B-cell population is important for the development of autoimmunity. *Blood* **118**, 1305–1315.
- Rubtsov, A.V., Rubtsova, K., Kappler, J.W., and Marrack, P. (2013). TLR7 drives accumulation of ABCs and autoantibody production in autoimmune-prone mice. *Immunol. Res.* **55**, 210–216.
- Rubtsova, K., Rubtsov, A.V., van Dyk, L.F., Kappler, J.W., and Marrack, P. (2013). T-box transcription factor T-bet, a key player in a unique type of B-cell activation essential for effective viral clearance. *Proc. Natl. Acad. Sci. USA* **110**, E3216–E3224.
- Rubtsova, K., Rubtsov, A.V., Cancro, M.P., and Marrack, P. (2015). Age-Associated B Cells: A T-bet-Dependent Effector with Roles in Protective and Pathogenic Immunity. *J. Immunol.* **195**, 1933–1937.
- Rubtsova, K., Rubtsov, A.V., Thurman, J.M., Mennona, J.M., Kappler, J.W., and Marrack, P. (2017). B cells expressing the transcription factor T-bet drive lupus-like autoimmunity. *J. Clin. Invest.* **127**, 1392–1404.
- Sansonno, D., Lauletta, G., De Re, V., Tucci, F.A., Gatti, P., Racanelli, V., Boiocchi, M., and Dammacco, F. (2004). Intrahepatic B cell clonal expansions and extrahepatic manifestations of chronic HCV infection. *Eur. J. Immunol.* **34**, 126–136.
- Sathaliyawala, T., Kubota, M., Yudanin, N., Turner, D., Camp, P., Thome, J.J., Bickham, K.L., Lerner, H., Goldstein, M., Sykes, M., et al. (2013). Distribution and compartmentalization of human circulating and tissue-resident memory T cell subsets. *Immunity* **38**, 187–197. <https://doi.org/10.1016/j.immuni.2012.09.020>.
- Sehdev, A.E., and Dumler, J.S. (2003). Hepatic pathology in human monocytic ehrlichiosis. *Ehrlichia chaffeensis* infection. *Am. J. Clin. Pathol.* **119**, 859–865.
- Sheneman, L., Evans, J., and Foster, J.A. (2006). Clearcut: a fast implementation of relaxed neighbor joining. *Bioinformatics* **22**, 2823–2824.
- Sonoda, E., Pewzner-Jung, Y., Schwers, S., Taki, S., Jung, S., Eilat, D., and Rajewsky, K. (1997). B cell development under the condition of allelic inclusion. *Immunity* **6**, 225–233.
- Standaert, S.M., Yu, T., Scott, M.A., Childs, J.E., Paddock, C.D., Nicholson, W.L., Singleton, J., Jr., and Blaser, M.J. (2000). Primary isolation of *Ehrlichia chaffeensis* from patients with febrile illnesses: clinical and molecular characteristics. *J. Infect. Dis.* **181**, 1082–1088.
- Stephens, R., Ndungu, F.M., and Langhorne, J. (2009). Germinal centre and marginal zone B cells expand quickly in a second *Plasmodium chabaudi* malaria infection producing mature plasma cells. *Parasite Immunol.* **31**, 20–31.
- Stevenson, H.L., Jordan, J.M., Peerwani, Z., Wang, H.Q., Walker, D.H., and Ismail, N. (2006). An intradermal environment promotes a protective type-1 response against lethal systemic monocytotropic ehrlichial infection. *Infect. Immun.* **74**, 4856–4864.
- Stone, S.L., Peel, J.N., Scharer, C.D., Risley, C.A., Chisolm, D.A., Schultz, M.D., Yu, B., Ballesteros-Tato, A., Wojciechowski, W., Mousseau, B., Misra, R.S., et al. (2019). T-bet Transcription Factor Promotes Antibody-Secreting Cell Differentiation by Limiting the Inflammatory Effects of IFN- γ on B Cells. *Immunity* **50**, 1172–1187.
- Thirumalapura, N.R., Stevenson, H.L., Walker, D.H., and Ismail, N. (2008). Protective heterologous immunity against fatal ehrlichiosis and lack of protection following homologous challenge. *Infect. Immun.* **76**, 1920–1930.
- Thirumalapura, N.R., Crossley, E.C., Walker, D.H., and Ismail, N. (2009). Persistent infection contributes to heterologous protective immunity against fatal ehrlichiosis. *Infect. Immun.* **77**, 5682–5689.
- Tsioris, K., Gupta, N.T., Ogunniyi, A.O., Zimnisky, R.M., Qian, F., Yao, Y., Wang, X., Stern, J.N., Chari, R., Briggs, A.W., et al. (2015). Neutralizing antibodies against West Nile virus identified directly from human B cells by single-cell analysis and next generation sequencing. *Integr. Biol.* **7**, 1587–1597.
- Urban, B.C., Hien, T.T., Day, N.P., Phu, N.H., Roberts, R., Pongponratn, E., Jones, M., Mai, N.T., Bethell, D., Turner, G.D., et al. (2005). Fatal *Plasmodium falciparum* malaria causes specific patterns of splenic architectural disorganization. *Infect. Immun.* **73**, 1986–1994.
- Weller, S., Braun, M.C., Tan, B.K., Rosenwald, A., Cordier, C., Conley, M.E., Plebani, A., Kumararatne, D.S., Bonnet, D., Tourmilhac, O., et al. (2004). Human blood IgM “memory” B cells are circulating splenic marginal zone B cells harboring a prediversified immunoglobulin repertoire. *Blood* **104**, 3647–3654.
- William, J., Euler, C., Christensen, S., and Shlomchik, M.J. (2002). Evolution of autoantibody responses via somatic hypermutation outside of germinal centers. *Science* **297**, 2066–2070.
- Winslow, G.M., Yager, E., Shilo, K., Volk, E., Reilly, A., and Chu, F.K. (2000). Antibody-mediated elimination of the obligate intracellular bacterial pathogen *Ehrlichia chaffeensis* during active infection. *Infect. Immun.* **68**, 2187–2195.
- Winslow, G.M., Papillion, A.M., Kenderes, K.J., and Levack, R.C. (2017). CD11c⁺ T-bet⁺ memory B cells: Immune maintenance during chronic infection and inflammation? *Cell. Immunol.* **321**, 8–17.
- Yates, J.L., Racine, R., McBride, K.M., and Winslow, G.M. (2013). T cell-dependent IgM memory B cells generated during bacterial infection are required for IgG responses to antigen challenge. *J. Immunol.* **191**, 1240–1249.

STAR★METHODS

KEY RESOURCES TABLE

REAGENT or RESOURCE	SOURCE	IDENTIFIER
Antibodies		
Rat anti B220 (clone: RA3 6B2) PerCPCy5.5	BD Biosciences	Catalog # 561101; RRID: AB_10565970
Rat anti CD19 (clone 1D3) FITC	BD Biosciences	Catalog # 553785; RRID: AB_395049
Rat anti IgM (clone B7-6) A488	Prepared in the lab	N/A
Rat anti CD21 (clone 7G6) A488	Prepared in the lab	N/A
Rat anti CD23 (clone B3B4) PE	eBioscience	Catalog # 12-0232-82; RRID: AB_465595
Rat anti CD4 (clone GK1.5) BV421	Biolegend	Catalog # 100401; RRID: AB_10900241
Hamster anti TCR- β (clone H57-597) PECy7	Biolegend	Catalog # 109222
Rat anti CD138 (clone 281-2) APC	Biolegend	Catalog # 142506; RRID: AB_10960141
Rat anti CD44 (IM7) APCCy7	Biolegend	Catalog # 103028; RRID: AB_830785
Rat anti CD73 (clone TY-11.8) bi	Biolegend	Catalog # 127204; RRID: AB_1089062
Hamster anti CD80 (clone 16-10A1) APC	eBioscience	Catalog # 16-0801-82; RRID: AB_467348
Rat anti PD-L2 (clone TY25) PE	eBioscience	Catalog # 12-5986-82; RRID: AB_466845
Hamster anti CD95 (clone Jo2) PECy7	BD Biosciences	Catalog # 557653; RRID: AB_27399999
Rat anti CD169 (clone 3D6.112) A647	Biolegend	Catalog # 142402; RRID: AB_2563620
Anti CD11b (clone M1-70) APCCy7	Biolegend	Catalog # 101214; RRID: AB_830641
Anti CD11c (clone N418) A647	eBioscience	Catalog # 14-0114-82; RRID: AB_469346
Anti CD69 (H1.2F3) PE	eBioscience	Catalog # 12-0691-82; RRID: AB_467326
Rat anti AID (clone mAID2) bi	eBioscience	Catalog # 14-5959-82; RRID: AB_468662
Anti T-bet (clone 4B10) PECy7	Biolegend	Catalog # 644824; RRID: AB_2561760
Bacterial and Virus Strains		
<i>Ehrlichia muris</i>	This paper and Thirumalapura et al., 2009	N/A
Chemicals, Peptides, and Recombinant Proteins		
<i>E. muris</i> antigens Omp 12 and Omp 19	This paper and Crocquet-Valdes et al., 2011	N/A
PNA	Vector laboratories and conjugated in the lab	Catalog # L1070; RRID: AB_2315097

(Continued on next page)

Continued

REAGENT or RESOURCE	SOURCE	IDENTIFIER
Oligonucleotides		
5-GGGAATTCGAGGTGCAGCTGCAG-3	This paper and Di Niro et al., 2015	N/A
5-TGCGAAGTCGACGCTGAGGAGACGGTGACCGTGG-3		
5-TGCGAAGTCGACGCTGAGGAGACTGTGAGAGTGG-3		
5-TGCGAAGTCGACGCTGCAGAGACAGTGACCAGAG-3		
5-TGCGAAGTCGACGCTGAGGAGACGGTGACTGAGG-3		
5-GGGAATTCGAGGTGCAGCTGCAGGAGTCTGG-3		
5- TGGTCCCTGTGCCCCAGACATCG –3		
5- GTGGTGCCTTGCCCCAGTAGTC –3		
5- AGAGTCCCTTGCCCCAGTAAGC –3		
5- GAGGTTCCCTTGCCCCAGTAGTC –3		
Critical Commercial Assays		
Click IT Plus Edu kit	ThermoFisher	Catalog # C10634
Ni NTA Spin kit	QIAGEN	Catalog # 31314
RNeasy plus micro kit	QIAGEN	Catalog # 74034
Zero Blunt PCR Cloning kit	ThermoFisher	Catalog # 450031
Deposited Data		
V region HTS data	NCBI Sequence Read Archive	BioProject PRJNA587455
mRNA-seq data	Gene Expression Omnibus database	GEO: GSE137154
Experimental Models: Organisms/Strains		
C57BL/6 mice	Jackson Laboratories	Catalog # 000664
B18+/- C57BL/6 mice	This paper and Sonoda et al., 1997	N/A
B18+/- Vk8R+/- C57BL/6 mice	This paper and Sonoda et al., 1997	N/A
huCD20 TamCre C57BL/6 mice	This paper and Khalil et al., 2012	N/A
Tbx21fl/fl C57BL/6 mice	This paper and Intlekofer et al., 2008	N/A
huCD20 TamCre Tbx21fl/fl C57BL/6 mice	This paper	N/A
B18+/- Vk8R+/- CD45.1/2 C57BL/6 mice	This paper	N/A
Software and Algorithms		
Flow Jo version 10	Flow Jo	https://www.flowjo.com/ ; RRID: SCR_008520
GraphPad Prism 7	GraphPad	https://www.graphpad.com/scientific-software/prism/ ; RRID: SCR_002798
IMGT V quest	IMGT	http://www.imgt.org/ ; RRID: SCR_012780
MUSCLE	European Bioinformatics	https://www.ebi.ac.uk/Tools/msa/muscle/ ; RRID: SCR_011812
FastQC v0.11.7	Babraham Institute	https://www.bioinformatics.babraham.ac.uk/projects/fastqc/ ; RRID: SCR_014583
Trimgalore v0.3.8	Babraham Institute	https://www.bioinformatics.babraham.ac.uk/projects/trim_galore/ ; RRID: SCR_016946
cutadapt v1.18	Babraham Institute	https://github.com/marcelm/cutadapt/ ; RRID: SCR_011841
STAR v2.6.1a	Dobin et al., 2013	https://github.com/alexdobin/STAR

(Continued on next page)

Continued

REAGENT or RESOURCE	SOURCE	IDENTIFIER
Subread v1.6.2; featureCounts	Liao et al., 2014	http://subread.sourceforge.net/ ; RRID: SCR_009803
Limma v3.20.9-voom	Law et al., 2014; Ritchie et al., 2015	https://ucdavis-bioinformatics-training.github.io/2018-June-RNA-Seq-Workshop/thursday/DE.html ; RRID: SCR_010943
Limma v3.20.9-rankSumTestWithCorrelation	Barry et al., 2008	https://www.rdocumentation.org/packages/limma/versions/3.28.14/topics/rankSumTestWithCorrelation ; RRID: SCR_010943
ImmuneDB v0.24.0	Rosenfeld et al., 2018	https://immunedb.readthedocs.io/en/latest/ ; RRID: SCR_017125

LEAD CONTACT AND MATERIALS AVAILABILITY

Requests for resources and reagents should be directed to and will be fulfilled by the Lead Contact for this study, Mark Shlomchik (mshlomch@pitt.edu).

EXPERIMENTAL MODEL AND SUBJECT DETAILS

The mice used in this study were bred under specific pathogen free conditions in the animal facility at the University of Pittsburgh. All mouse work was done according to the protocols approved by the University of Pittsburgh Institutional Animal Care and Use Committee. The following mouse strains were used: *C57BL/6* (Jackson Laboratories), *B18+/+* and *B18+/+ Vk8R+/+* (Sonoda et al., 1997), *huCD20 TamCre* (Khalil et al., 2012), *Tbx21fl/fl* (Intlekofer et al., 2008), *huCD20 TamCre Tbx21fl/fl*, and *B18+/- Vk8R+/- CD45.1/2*. *E. muris* was used for infection of the above-mentioned mouse strains (Thirumalapura et al., 2009).

METHOD DETAILS**Infection and Treatment Procedures**

E. muris infections were done according to procedures described previously (Stevenson et al., 2006; Thirumalapura et al., 2009). Briefly, *E. muris* inoculum was prepared by passage through wild-type *C57BL/6* carrier mice. Single cell suspensions from spleens harvested from carrier mice were used for infection of experimental mice. Mice were infected intraperitoneally with 10^5 *E. muris*/mouse (Thirumalapura et al., 2009). The bacterial burden was assessed by quantitative RT-PCR as described previously (Stevenson et al., 2006). Tamoxifen treatments were done at day 3, 5 and 7 post infection at a dose of 1 or 2 mg orally in corn oil. For labeling B cells in the circulation, 1 μ g CD19 PE was injected intravenously. After 3 min, blood, spleen and liver were harvested and analyzed. For MBC homing experiments, CD45.2 MBC subsets were FACS sorted, CFSE labeled and transferred intravenously into *B18+/- Vk8R+/- CD45.1/2* mice.

ELISpot Assays

Single cell suspensions from spleen were obtained by mechanical disruption of the tissue, followed by treatment with ACK buffer for lysis of red blood cells. Single cell suspension of the liver was prepared by mechanical disruption using the MACS dissociator along with use of 50KU/mL DNase and collagenase 100U/mL, followed by treatment with ACK buffer for lysis of red blood cells. The single cell suspension from the liver was re-suspended in 20% Percoll and underlaid with 80% Percoll. The Percoll gradient was spun at 450 rcf for 20 min at room temperature. The lymphocytes were collected from the interface of the Percoll gradients and washed with media before further use in various assays described below. For ELISpot assay, Immulon 4-HBX plates were coated with the following antigens: anti-kappa at 5 mg/mL, *Omp12* at 4mg/mL and *Omp19* at 4mg/mL. *E. coli* strains containing recombinant plasmids for *E. muris* antigens *Omp 12* and *Omp 19* were provided by David Walker at University of Texas Medical Branch (Crocquet-Valdes et al., 2011). The recombinant His tagged proteins were produced and purified using Ni-NTA spin kit from QIAGEN as per standard protocols (Crocquet-Valdes et al., 2011). For ELISpot assay, non-specific binding was blocked with 1% bovine serum albumin (BSA) in PBS. Splenocytes were incubated overnight at 37°C. AFC were detected by using alkaline phosphatase-conjugated secondary Ab (to IgG or IgM, Southern Biotech) and 5-bromo-4-chloro-3-indolyl-phosphate in agarose.

Flow Cytometry

For FC staining, non-specific binding was blocked using anti-FcR clone 2.4G2 and dead cells were excluded using cell viability dye (Tonbo Biosciences). The Abs were either purified in our lab or purchased and are as follows. Anti-B220 (Biolegend, RA3-6B2), anti-CD19 (BD ID3), anti-IgM (homemade, B7-6), anti-CD45 (home-made 30-F11), anti-CD21 (homemade, 7G6), anti-CD23 (ebioscience,

B3B4) for B cells, anti-CD4 (Biolegend, GK1.5), anti-TCR- β (Biolegend H57-597) for T cells, anti-CD138 (Biolegend, 281-2) and anti-CD44 (Biolegend, IM7) for B cell blasts and PB, anti-CD73 (Biolegend, TY-11.8), anti-CD80 (ebioscience, 16-10A1), anti-PD-L2 (ebioscience, TY25) for MBC, PNA (vector labs), anti-CD95 (BD, Jo2) for GCBC, anti-CD169 (Biolegend, 3D6.112) for metallophilic macrophages, anti-CD11b (Biolegend M1-70), anti-CD11c (ebioscience, N418), anti-CD69 (ebioscience, H1.2F3), anti-AID (ebioscience, mAID-2) and anti-T-bet (Biolegend, 4B10). The click IT Plus Edu kit was purchased from Invitrogen and the staining was done according to the recommended protocol. The cells were analyzed on LSR II or Fortessa instruments (BD) and the data were analyzed on FlowJo software.

Immunofluorescence imaging

7 mm spleen sections were prepared from OCT-frozen tissues, fixed in acetone for 10 min, and stored at -80°C . The slides were thawed and re-hydrated using PBS and blocked using PBS+1% BSA and 2.4G2 for 10 min. The slides were then stained with relevant Abs as described in the figure legends in a dark humid chamber for 30 min. The Abs were either purified in our lab or purchased and are as follows. Anti-B220 (Biolegend RA3-6B2), anti-CD19 (BD ID3), anti-IgM (home-made B7-6), for B cells, anti-CD4 (Biolegend GK1.5), anti-TCR- β (Biolegend H57-597) for T cells, anti-CD138 (Biolegend 281-2) for PB, anti-CD169 (Biolegend 3D6.112) for metallophilic macrophages, anti-CD11c (ebioscience N418) and anti-T-bet (Biolegend 4B10). The slides were washed thrice using PBS and the same steps were followed for secondary Ab. For intracellular staining, the sections were permeabilized using 0.3% Triton X-100 reagent before staining. Sections were mounted using ProLong Anti-fade Gold (Life Technologies) and imaged using Olympus Fluorescence Microscope IX3-BSW and acquired using Cell Sens Dimension software.

V region sequencing

V region sequencing was done on FACS sorted PB or micro-dissected B cell patches. 7 mm spleen sections were prepared from OCT-frozen tissues on the membrane-coated PEN slides (Leica). PB patches were detected using anti-IgM Alexa488 staining. Microdissections were performed using Zeiss PALM MicroBeam Laser Capture Microdissection System. Dissected patches were collected in the cap of PCR microtubes in 12 μL of digestion buffer (50 mM Tris-HCl, 50 mM KCl, 0.63 mM EDTA, 0.22% Igepal, 0.22% Tween20, 0.8 mg/mL proteinase K). The patches or FACS sorted PB were digested at 37°C for 4 h and then at 90°C for 5 min. Primers, V region amplification and data analysis has been described previously (Di Niro et al., 2015). Briefly, a primary PCR was performed using the primers MsVHE-short: 5-GGGAATTCGAGGTGCAGCTGCAG-3 and a mix of 4 JH region anti-sense primers 3 Sall P-mJH01: 5-TGCGAAGTCGACGCTGAGGAGACGGTGACCGTGG-3 3SallP-mJH02: 5-TGCGAAGTCGACGCTGAGGAGACTGTGAGAGTGG-3 3SallP-mJH03: 5-TGCGAAGTCGACGCTGCAGAGACAGTGACCAGAG-3 3SallP-mJH04: 5-TGCGAAGTCGACGCTGAGGAGACGGTGACTGAGG-3. A second nested PCR was performed using 1 μL of the product from the 1st PCR using the primers MsVHE: 5-GGGAATTCGAGGTGCAGCTGCAGGAGTCTGG-3 and a mix of JH antisense primers 5'- TGGTCCCTGTGCCCCAGACATCG -3', 5'- GTGGTGCCTTGCCCCAGTAGTC -3', 5'- AGAGTCCCTTGCCCCAGTAAAGC -3' and 5'- GAGGTTCCCTTGACCCAGTAGTC -3'. High fidelity polymerase Pfu Turbo (Agilent) was used for the PCR amplification to minimize the possibility of PCR error while generating the V region sequence. The resulting PCR products were cloned and sequenced using Zero Blunt PCR cloning kit (ThermoFisher). Sequence analysis was done by using http://www.imgt.org/IMGT_vquest/analysis.

Cell Sorting and RNA preparation

PB were sorted as TCR- β negative, CD138 positive, CD44 positive, CD19 intermediate, B cell blasts were sorted as TCR- β negative, CD44 positive, CD138 negative, CD19 positive, naive B cells were sorted as CD19 positive, CD138 negative and CD44 negative, CD73 negative. For HTS, B cells were sorted from naive mice as CD45 positive, CD19 positive, CD73 negative, and MBC were sorted from memory mice as CD45 positive, CD19 positive and CD73 positive. For mRNA sequencing analysis, B220 positive, CD73 positive MBC were sorted as CD11b, CD11c double negative and CD11b, CD11c double positive from memory mice. The staining was done as described earlier for FC. After sorting, cells were spun down and washed with PB and re-suspended in RLT+1% beta-mercaptoethanol. RNA was prepared with RNeasy microplus kits from QIAGEN, according to recommended protocol.

HTS library preparation and analysis

For HTS, B cell blasts, PB, and MBC were FACS sorted and RNA was prepared as described above. The method for high-throughput sequencing of the B cell repertoire was performed as previously described (Di Niro et al., 2015; Tsioris et al., 2015). Briefly, RNA was reverse-transcribed into cDNA using a biotinylated oligo dT primer. An adaptor sequence was added to the 3' end of all cDNA, which contains the Illumina P7 universal priming site and a 17-nucleotide unique molecular identifier (UMI). Products were purified using streptavidin-coated magnetic beads followed by a primary PCR reaction using a pool of primers targeting the IGHA, IGHD, IGHE, IGHG, IGHM, IGKC and IGLC regions, as well as a sample-indexed Illumina P7C7 primer. The immunoglobulin-specific primers contained tails corresponding to the Illumina P5 sequence. PCR products were then purified using AMPure XP beads. A secondary PCR was then performed to add the Illumina C5 clustering sequence to the end of the molecule containing the constant region. The number of secondary PCR cycles was tailored to each sample to avoid entering plateau phase, as judged by a prior quantitative PCR analysis. Final products were purified, quantified with Agilent TapeStation and pooled in equimolar proportions, followed by high-throughput paired-end sequencing on the Illumina MiSeq platform. For sequencing, the Illumina 600 cycle kit was used with the modifications that 325 cycles were used for read 1, 6 cycles for the index reads, 300 cycles for read 2 and a 20% PhiX spike-in to increase sequence diversity.

FASTA files provided by Juno were analyzed with ImmuneDB v0.24.0 using default parameters for all stages (Rosenfeld et al., 2018). The GL reference sequences were acquired from IMGT's GENE-DB, which can be accessed at <http://www.imgt.org/IMGIndex/IMGGene-db.php>. After clonal assignment, lineages were generated with clearcut (Sheneman et al., 2006) using neighbor-joining, excluding mutations that occurred in only one sequence. Data were then exported from ImmuneDB for downstream analysis. Clones were included in this analysis only if they had between 1 and 4 non-templated CDR3 residues (as measured from the first non-GL-encoded nucleotide) or at least 4 common V-gene mutations across all sequences. ETE3 v3.1.1 (Huerta-Cepas et al., 2016) was used to calculate tree metrics and numpy v1.15.0 was used for all statistical testing. The HTS data generated during this study are available in the NCBI's Sequence Read Archive (SRA) with accession ID BioProject: PRJNA587455.

RNA seq analysis

MBC were FACS sorted and RNA was prepared as described above. cDNA libraries were constructed using SMARTer low input kit for mRNA seq (Clontech). Samples were sequenced using Illumina NextSeq 500 with 75 bp paired-end reads and aligned to the mm10 genome using the STAR aligner (Dobin et al., 2013). The number of uniquely aligned reads ranged from 22 to 32 million. Gene-level counts were determined using featureCounts (Liao et al., 2014), and raw counts were quantile normalized to each other for differential expression using the voom method (Law et al., 2014) in the limma R package (Ritchie et al., 2015). The presence of certain liver-specific transcripts indicated unavoidable liver cell contamination in the liver sample; to prevent this from confounding our analysis, differential expression was performed only on genes, which were having at least 30 counts in the all liver and spleen samples. All RNA-seq data were deposited in the NCBI's Gene Expression Omnibus database (GEO) with accession ID GSE137154. All gene-set enrichments were performed using the rankSumTestWithCorrelation function in limma, which explicitly corrects for correlation among genes in the gene set being interrogated. For differential analysis of splenic and liver memory subsets in figure S7, the naive B cell transcriptional profile was extracted from a previously published microarray study (Barnett et al., 2016). For normalization of the datasets, the Quantile method was used.

QUANTIFICATION AND STATISTICAL ANALYSIS

Statistical analysis was performed with Prism (GraphPad Software). p values were determined using Student's t tests (two-tailed). For multiple comparisons, Two-Way ANOVA or Mann Whitney tests or Chi square analysis were applied. Differences between groups were considered significant for p values < 0.05 (* p < 0.05; ** p < 0.01; *** p < 0.001; **** p < 0.0001).

DATA AND CODE AVAILABILITY

The RNA seq data generated during this study is available in the NCBI's Gene Expression Omnibus database (GEO) with accession ID GEO: GSE137154. The HTS data generated during this study are available in the NCBI's Sequence Read Archive (SRA) with accession ID BioProject: PRJNA587455.